NUREG/CR-1709
ORNL/NUREG/CSD/TM-17

UCC-ND

NUCLEAR DIVISION

UNION CARBIDE

MASTER

ORMDIN: A Finite Element Program for Two-Dimensional Nonlinear Inverse Heat Conduction Analysis

B. R. Bass
J. B. Drake
L. J. Ott

Prepared for the U.S. Nuclear Regulatory Commission
Office of Nuclear Regulatory Research
Under Interagency Agreements DOE 40-551-75 and 40-552-75

OPERATED BY
UNION CARBIDE CORPORATION
FOR THE UNITED STATES
DEPARTMENT OF ENERGY

DISCLAIMER

The following pages are an exact representation of what is in the original document folder.

Printed in the United States of America. Available from
National Technical Information Service
U.S. Department of Commerce
5285 Port Royal Road, Springfield, Virginia 22161

Available from

GPO Sales Program
Division of Technical Information and Document Control
U.S. Nuclear Regulatory Commission
Washington, D.C. 20555

NUREG/CR-1709
ORNL/NUREG/CSD/TM-17
Dist. Category R2

ORMDIN: A FINITE ELEMENT PROGRAM FOR TWO-DIMENSIONAL NONLINEAR INVERSE HEAT CONDUCTION ANALYSIS

B. R. Bass
J. B. Drake
L. J. Ott*

Sponsor: J. D. White

Manuscript Completed: September 1980
Date Published: December 1980

Prepared for the
Office of Nuclear Regulatory Research
U. S. Nuclear Regulatory Commission
Washington, DC 20555
Under Interagency Agreements DOE 40-551-75 and 40-552-75

NRC FIN No. B0125

COMPUTER SCIENCES DIVISION
at
Oak Ridge Gaseous Diffusion Plant
Post Office Box P
Oak Ridge, Tennessee 37830

*Engineering Technology Division, Oak Ridge National Laboratory, Oak Ridge, TN 37830.

Union Carbide Corporation, Nuclear Division
operating the
Oak Ridge Gaseous Diffusion Plant . Oak Ridge National Laboratory
Oak Ridge Y-12 Plant . Paducah Gaseous Diffusion Plant
under Contract No. W-7405-eng-26
for the
Department of Energy

THIS PAGE

WAS INTENTIONALLY

LEFT BLANK

TABLE OF CONTENTS

ACKNOWLEDGMENTS

This work was supported by the Nuclear Regulatory Commission through the Oak Ridge National Laboratory Pressurized-Water Reactor Blowdown Heat Transfer Separate-Effects Program.

LIST OF FIGURES

LIST OF FIGURES (Contd)

LIST OF SYMBOLS

Symbol	Definition
a	Radius of cylindrical rod
[A]	Matrix, as defined in equation (33)
[B]	Matrix, equation (10)
[C]	Heat capacity matrix for assembly of elements
{D}	Vector, equation (34)
c	Specific heat
e	Index of elements
E	Number of elements in assembly
$\{\overline{F}\}$	Vector for assembly of elements, equation (11)
$\{\bar{\bar{F}}\}$	Vector for assembly of elements, equation (12)
h	Convective heat transfer coefficient
h^r	Radiative heat transfer coefficient, equation (5)
J	Number of time steps in analysis interval; J - 1 equals number of "future" temperatures
[K]	Thermal conductivity matrix for assembly of elements
k	Thermal conductivity
L	Number of interior temperature probes; also, number of nodes in surface heat flux interpolation
M	Number of nodes in temperature interpolation
N_I	Interpolation function for temperature
{N}	Vector of interpolation functions for temperature
$\underline{n}$	Unit outward normal to boundary surface
Q	Internal heat generation rate, per unit volume
q	Imposed surface heat flux
q_ℓ	Value of surface heat flux at ℓ^{th} node, equation (22)

LIST OF SYMBOLS (Contd.)

Symbol	Definition
$\{q\}$	Surface heat flux vector of dimension L, equation (22)
q^c	Surface heat flux due to convection
q^r	Surface heat flux due to radiation
R_ℓ	Interpolation function for surface heat flux
$\{R\}$	Vector of interpolation functions for surface heat flux
r	Radial coordinate
r^p	Radial coordinate of temperature probe location
$[S]$	Matrix, as defined in equation (17)
T	Temperature
T_I	Value of temperature at Ith node
$\{T\}$	Temperature vector
T_ℓ^p	Measured temperature at internal point (r^p, θ_ℓ)
T^{ac}	Temperature at which no convection occurs
T^{ar}	Temperature at which no radiation occurs
T^w	Temperature at wall
t	Time
TOL1	Convergence tolerance for temperature vector, equation (19)
TOL2	Convergence tolerance for surface heat flux, equation (35)
w_j	Weighting functions, equation (27)
$\underline{x}$	General spatial coordinates

LIST OF SYMBOLS (Contd.)

Symbol	Definition
α	Thermal diffusivity
ρ	Density
Ω	General spatial domain
Ω^e	Element domain
Γ_1	Boundary on which condition (2) is prescribed
Γ_2	Boundary on which condition (3) is prescribed
Γ_2^e	Element external boundary on which condition (3) is prescribed
∇	Gradient operator
σ	Stefan-Boltzmann constant
ε	Emissivity
β	Surface heat flux parameter, equation (25)
Δ	Incremental change in kernel
θ	Angular coordinate
θ_ℓ	Angular coordinate of ℓ^{th} temperature probe and related surface heat flux node
ϕ	Sensitivity coefficient, equation (30)
λ	Perturbation factor for q_ℓ, equation (30)
τ	Dimensionless time
$\sum$	Summation symbol

Subscripts

I	Index of nodes
i	Index of time steps in solution, where i is a non-negative integer
j	Index of time steps in analysis interval, $1 \leq j \leq J$

LIST OF SYMBOLS (Contd.)

Subscripts	Definition
k,ℓ,m	Index of nodes for temperature probes and surface heat flux nodes
$(i)\Delta t$ or $;(i)\Delta t$	Time $t = (i)\Delta t$ at which kernel is evaluated
Superscripts	
$[\ ]^T$	Transpose of matrix
$\{\ \}^T$	Row vector
$(P),(H)$	Iteration number at which kernel is evaluated
Other Symbols	
$[\ ]$	Matrix
$\{\ \}$	Column vector
$\|\|\ \|\|$	Euclidean norm
$\int$	Integral sign

ORMDIN: A FINITE ELEMENT PROGRAM FOR TWO-DIMENSIONAL NONLINEAR INVERSE HEAT CONDUCTION ANALYSIS

B. R. Bass
J. B. Drake
L. J. Ott

ABSTRACT

The calculation of the surface temperature and surface heat flux from measured temperature transients at one or more interior points of a body is identified in the literature as the inverse heat conduction problem. Heretofore, analytical and computational methods of treating this problem have been limited to one-dimensional nonlinear or two-dimensional linear material models. This report presents, to the authors' knowledge, the first inverse solution technique applicable to the two-dimensional nonlinear model with temperature-dependent thermophysical properties. This technique, representing an extension of the one-dimensional formulation previously developed by one of the authors, utilizes a finite element heat conduction model and a generalization of Beck's one-dimensional nonlinear estimation procedure. A digital computer program ORMDIN (Oak Ridge Multi-Dimensional INverse) is developed from the formulation and applied to the cross section of a composite cylinder with temperature-dependent material properties. Results are presented to demonstrate that the inverse formulation is capable of successfully treating experimental data. An important feature of the method is that small time steps are permitted while avoiding severe oscillations or numerical instabilities due to experimental errors in measured data.

I. INTRODUCTION

The Oak Ridge National Laboratory (ORNL) Pressurized-Water Reactor (PWR) Blowdown Heat Transfer (BDHT) Program [1] is an experimental separate-effects study of the principal phenomena that are important to loss-of-coolant accident (LOCA) analysis. Primary test results are obtained from the Thermal-Hydraulic Test Facility (THTF), a large non-nuclear experimental loop with a test section that contains an array of indirect electrically heated fuel pin simulators with a 365.76 cm (12 ft) heated length.

One of the primary objectives of the ORNL BDHT separate-effects program is the determination of the transient surface temperature and surface heat flux of fuel pin simulators (FPS) from internal thermocouple signals obtained during a loss-of-coolant experiment (LOCE) in the THTF. This analysis requires the solution of the classical inverse heat conduction problem. The state-of-the-art solution of the inverse heat conduction problem [2,3] is one-dimensional in scope; that is, for an FPS cylindrical geometry, it is normally assumed that azimuthal and axial heat conduction are negligible, thereby allowing the governing differential equation to be reduced to one dimension in terms of radius only.

Analysis [4] has shown that these assumptions can introduce significant errors in the computed surface heat flux and surface temperature. The fuel pin simulators in the first rod bundle used in the THTF had a dual-sheath design (see idealized rod cross section in Figure 1) with thermocouples (those used for the inverse computations) being located in axial grooves machined in the inner sheath. These FPSs

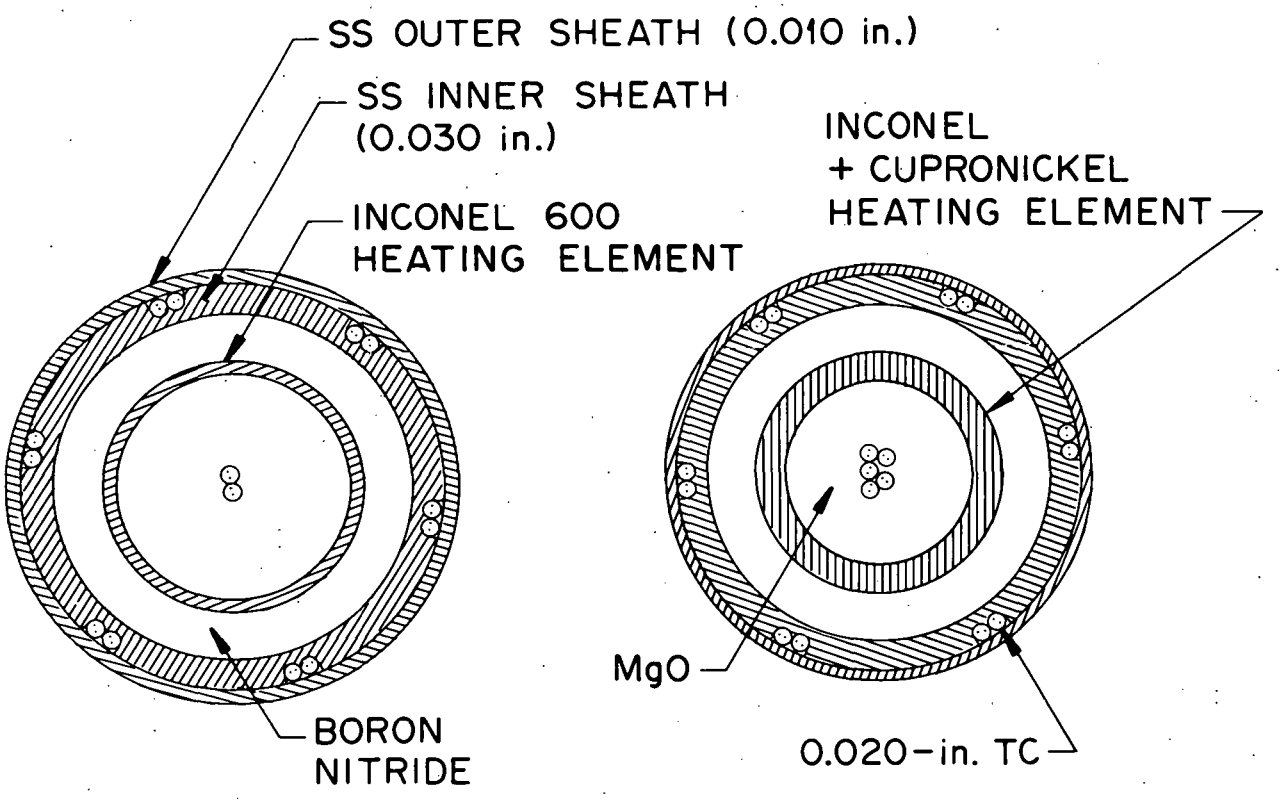

Figure 1. Idealized representation of THTF bundle 1 FPS

were reduced to their final outside diameter by swaging; this operation crushed the embedded thermocouples to a somewhat elliptical shape and pulled the edges of the milled groove away from the outer sheath, thus forming air pockets around the thermocouples. Two-dimensional modeling of these BDHT fuel pin simulators using HEATING5 [5], a generalized heat conduction code developed at ORNL, revealed severe perturbations in the surface heat flux and temperature driving potential. Figure 2 typifies these HEATING5 simulation results which illustrated a surface flux depression in the vicinity of the thermocouple and groove (as much as 7% - 23% less than the mean flux) and surface flux rise away from the groove (4% - 7% greater than the mean flux). Eccentricity of the heating element with respect to the outer sheaths contributed an extra $\pm$ 12% perturbation in the computed surface conditions. Thus, it was concluded that azimuthal heat conduction could not be neglected. Additional work revealed that axial conduction could be neglected if the location to be analyzed was at least 2.54 cm distant (axially) from a change in power generation rate.

Problem areas in the bundle 1 fuel pin simulators, highlighted by the above analysis effort [4], were essentially eliminated in the design and construction of the third bundle to be used in the THTF. Bundle 3 FPSs were constructed with a single outside sheath (rather than the dual-sheath of bundle 1), insulator preforms to minimize eccentricity, and multiple sheath thermocouples per axial level (as against one in bundle 1). HEATING5 analysis of this FPS design showed the surface heat flux to be perturbed by only $\pm$ 2% of the mean flux. X-rays and cross sections of prototypical bundle 3 FPSs revealed negligible eccentricity. Furthermore,

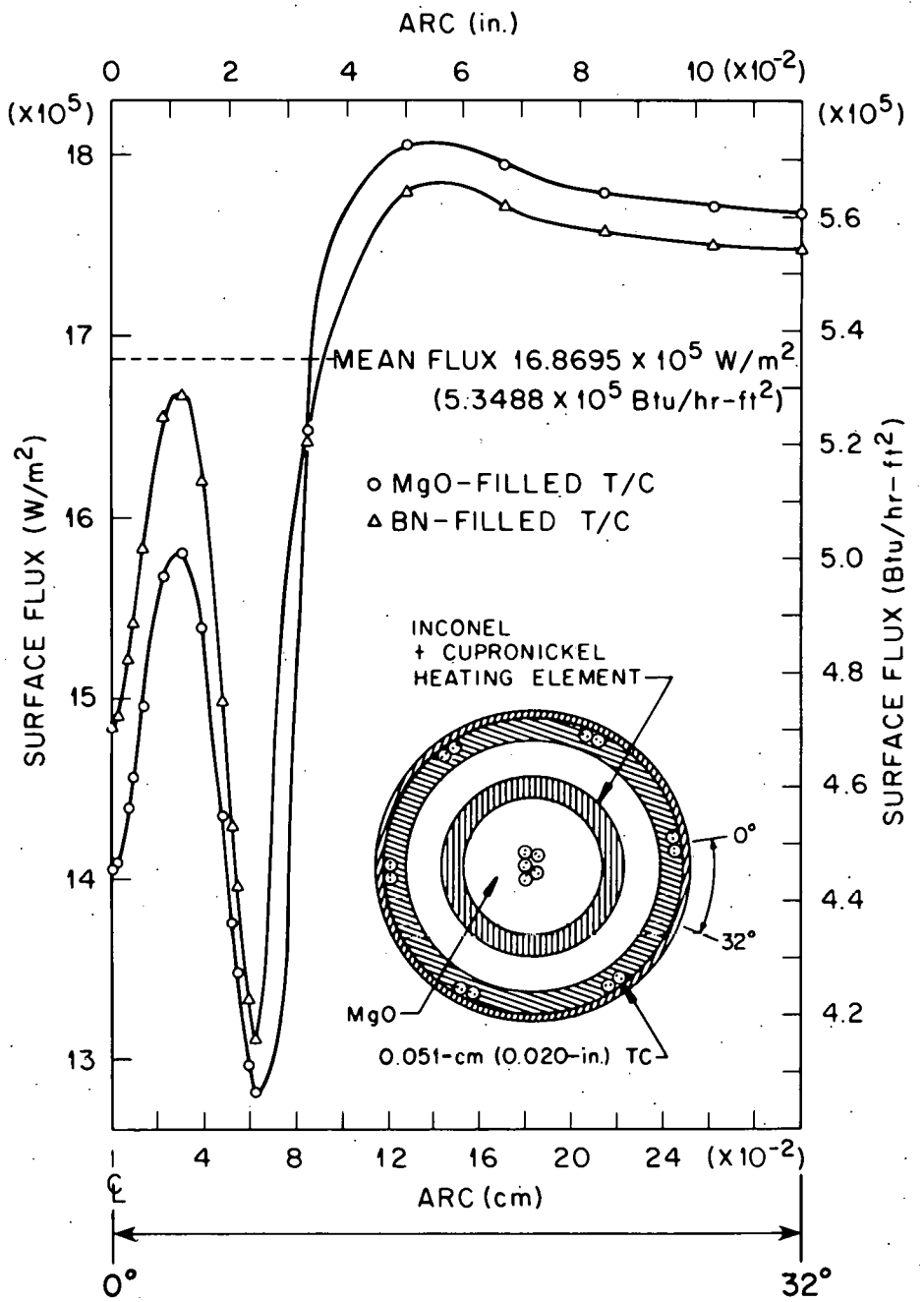

Figure 2. Surface heat flux perturbation in THTF bundle 1 FPS

the bundle 3 FPS incorporated a flat power profile (i.e., no changes in the power generation rate except at the ends of the 365.76 cm heated length). These bundle 3 fuel pin simulators were as nearly axisymmetric as possible using state-of-the-art manufacturing processes; and, therefore, axial and azimuthal heat conduction could possibly be neglected.

Experimental evidence, however, rules out the luxury of the above assumptions. Originally, the bundle 3 FPS design included three thermocouples per level so that eccentricity in the FPS could be detected simply from the thermometry. However, during LOCE tests of prototypical bundle 3 FPSs in a single rod test facility at ORNL, the three thermocouples indicated significant differences in the FPS surface behavior circumferentially at one axial level. For example, during blowdown FCTF 79-1-6, three thermocouples at axial level D exhibited behavior as shown in Figure 3. Thermocouples D1, D2, and D3 responded similarly during steady-state and the first 5 sec of the LOCE. However, the similarities ended starting with a sustained temperature excursion from D1 at 5.25 sec, D3 followed suit at 5.33 sec, but D2 (120° azimuthally from both D1 and D3 in an 0.95 cm-OD FPS) did not indicate CHF until 0.5 sec after D3. Also, thermocouple D3 showed a slight rewet at 5.64 sec before continuation of the temperature excursion at 5.75 sec. The extreme response differences in the FPS surface behavior cannot be explained by the design, construction or internals of the FPS. The differences in the circumferential surface behavior are attributed to forces purely external to the FPS (i.e., different fluid conditions). Therefore, even for a perfectly axisymmetric simulator, azimuthal heat conduction in the FPS cannot be neglected.

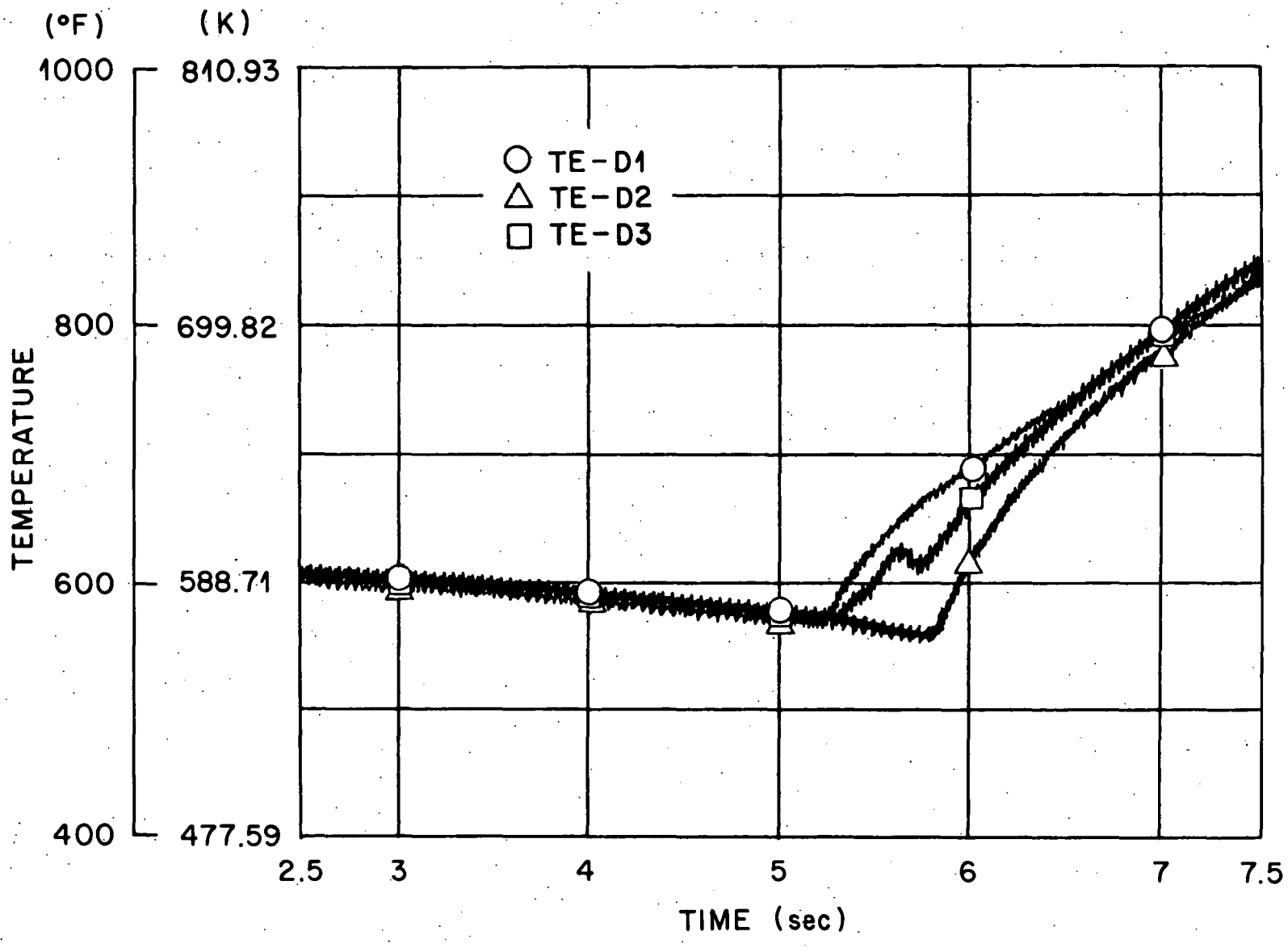

Figure 3. D level thermocouple responses during blowdown No. FCTF 79-1-6

These experimental observations indicate that determination of surface conditions of the bundle 3 FPS from interior thermocouple transients requires solution of a multidimensional inverse formulation. This requirement has motivated the initial development of a two-dimensional nonlinear inverse technique that models radial and azimuthal heat conduction in a composite cylinder. The following sections of this report describe the inverse technique, implementation of the technique in the digital computer program ORMDIN, and application of ORMDIN to transients recorded by the bundle 3 FPS in a representative FCTF blowdown.

II. OBJECTIVE

In heat transfer studies, a class of problems can be identified where the surface temperature and surface heat flux are determined from the temperature history measured at a set of discrete points in the interior of the body. Generally, this class is referred to in the literature as the inverse problem, in contrast with the usual direct formulation where the interior temperature history is determined from specified initial and boundary conditions. Typically, the inverse formulation arises in experimental studies where direct measurement of surface conditions is not feasible, such as convective heat transfer in rocket nozzles or quenching processes for materials. An application presented in this paper treats an electrically heated composite rod with two-phase flow boundary conditions. Temperature transients recorded by thermocouple probes in the rod are used to investigate the time history of surface conditions. Because these probes are positioned in the interior of the rod to avoid disturbing surface conditions and the flow adjacent to the surface, an inverse problem must be solved.

Various methods that have been applied to the inverse problem include integral equation solutions, series solutions, transform solutions, and function minimization techniques. Extensive bibliographies that survey these methods are readily available in the literature (see, for example, [6] and [7]); the limited number of references mentioned here deal with materially nonlinear or multidimensional inverse formulations. Heretofore, analytical and computational methods for treating the nonlinear inverse problem of temperature-dependent thermophysical properties have been restricted to one-dimensional models. Beck [7,8] has developed

a nonlinear formulation based on a finite difference heat conduction model and nonlinear estimation procedures. Muzzy et al. [9] and Bass [10] have applied Beck's method, with some modifications, to one-dimensional composite models with temperature-dependent material properties. Other nonlinear formulations include a finite difference technique developed by Ott and Hedrick [2] and a transform method by Imber [6]. Apparently, the only two-dimensional inverse formulation appearing in the open literature is that of Imber [11,12]. His transform technique is applicable to two-dimensional geometries of arbitrary shape, but assumes a linear material model with constant properties.

This report presents, to the authors' knowledge, the first inverse solution technique applicable to the two-dimensional nonlinear model with temperature-dependent properties. This technique, representing an extension of the one-dimensional formulation previously developed by Bass [10], utilizes a finite element heat conduction model and a generalization of Beck's one-dimensional nonlinear estimation procedure. The computational technique assumes several thermocouple sensors judiciously positioned in the interior of the material body. In the formulation, the unknown surface heat flux is discretized on the boundary domain of the body using a prescribed set of nodal points and suitable interpolating functions. Because the temperature response at interior locations is delayed and damped with respect to changes in surface conditions, these nodal point values of surface heat flux are determined in a given time step with a procedure that utilizes interior temperatures at "future" times. Specifically, the nodal values of flux are assumed to be constant or to vary piecewise linearly over an analysis interval that consists of several time steps

in the discretized data. The coefficients that describe the nodal values are adjusted iteratively to achieve the closest agreement in a least squares sense with the input "future" temperatures over the analysis interval. The discretized approximation of the surface heat flux thus determined provides a conventional boundary condition for the forward problem in the next time step. The inverse solution computed in this way represents a "best approximation" in the finite dimensional subspace of solutions defined by the surface heat flux interpolation. An important feature of the method is that small time steps are permitted while avoiding severe oscillations or numerical instabilities due to experimental errors in measured data.

The formulation is implemented in the digital computer program ORMDIN and applied to the cross section of a composite cylinder with temperature-dependent material properties. To evaluate the performance of the technique in solving the inverse problem, a standard initial-boundary value solution, with a known surface heat flux, is used as input for the inverse calculation. The computed surface heat flux is compared with the (known) imposed heat flux for two different thermocouple configurations. Finally, the technique is applied to experimentally determined temperature transients recorded at interior points of an electrically heated cylinder (THTF bundle 3 FPS) used to simulate a nuclear fuel rod in reactor loss-of-coolant analyses.

III. FINITE ELEMENT FORMULATION OF THE DIRECT PROBLEM

The conduction of heat in the region Ω is governed by the quasi-linear parabolic equation

$$\nabla \cdot (k\nabla T) + Q = \rho c \frac{\partial T}{\partial t} \tag{1}$$

subject to the boundary conditions

$$T = T^{w} \text{ on } \Gamma_1 \tag{2}$$

and

$$k\nabla T \cdot \underline{n} + q + q^{r} + q^{c} = 0 \text{ on } \Gamma_2 \quad . \tag{3}$$

The heat flow rates per unit area on convection and radiation boundaries are written

$$q^{c} = h(T - T^{ac}) \quad , \quad q^{r} = h^{r}(T - T^{ar}) \quad , \tag{4}$$

where h^{r} is defined by

$$h^{r} = \varepsilon\sigma(T^2 + T^{ar^2})\ (T + T^{ar}) \quad . \tag{5}$$

In general, k, c, h, and h^{r} are temperature and spatially dependent, while Q and q are time and spatially dependent.

Let the region Ω be partitioned by a system of finite elements and let the unknown temperature T be approximated throughout the solution domain at any time t by

$$T(\underline{x},t) = \sum_{I=1}^{M} N_I(\underline{x})\ T_I(t) = \{N\}^T \{T\} \quad . \tag{6}$$

Here the N_I are the interpolation functions defined piecewise element by element and the T_I or $\{T\}$ are the nodal temperatures. The governing equations of the discretized system can be derived by minimizing a functional or by using Galerkin's method [13]. In the Galerkin formulation employed here, the problem is recast in a weighted integral form using the interpolating functions N_I as the weighting functions:

$$\int_{\Omega^e} \{N\}[\nabla \cdot (k\nabla(\{N\}^T \{T\})) + Q - \rho c \frac{\partial}{\partial t} (\{N\}^T \{T\})] \, d\Omega$$

$$- \oint_{\Gamma_2{}^e} \{N\}[k\nabla(\{N\}^T \{T\}) \cdot \underline{n} + q + h(\{N\}^T \{T\} - T^{ac})$$

$$+ h^r(\{N\}^T \{T\} - T^{ar})] \, d\Gamma = 0 \quad . \tag{7}$$

Only a single finite element is considered in the integral (7), as the governing equations of the complete system of elements are obtained by assembling the individual finite element matrices. The surface integral over $\Gamma_2{}^e$ refers only to those elements with external boundaries on which condition (3) is given.

Green's first identity is applied to the first volume integral of equation (7) so that the second derivatives do not impose unnecessary continuity conditions between elements. When use is made of the boundary conditions (2) and (3), the integral formulation (7) leads to a set of transient ordinary differential equations for the assemblage of finite elements:

$$[C] \frac{\partial\{T\}}{\partial t} + [K] \{T\} + \{\overline{F}\} + \{\overline{\overline{F}}\} = 0 \quad . \tag{8}$$

The components in equation (8) are defined by:

$$[C] = \sum_{e=1}^{E} \int_{\Omega^e} \rho c \{N\} \{N\}^T \, d\Omega \quad , \tag{9}$$

$$[K] = \sum_{e=1}^{E} \int_{\Omega^e} k[B] [B]^T \, d\Omega + \sum_{e=1}^{E} \oint_{\Gamma_2{}^e} (h + h^r) \{N\} \{N\}^T \, d\Gamma \quad ,$$

$$[B] = \nabla\{N\} \quad , \tag{10}$$

$$\{\bar{F}\} = - \sum_{e=1}^{E} \int_{\Omega^e} \{N\} Q d\Omega + \sum_{e=1}^{E} \oint_{\Gamma_2{}^e} \{N\} q d\Gamma \quad , \tag{11}$$

$$\{\bar{\bar{F}}\} = - \sum_{e=1}^{E} \oint_{\Gamma_2{}^e} \{N\} (h^r T^{ar} + h T^{ac}) \, d\Gamma \quad , \tag{12}$$

where the summations are taken over the individual finite element contributions. These integrals are evaluated numerically using Gauss-Legendre quadrature in the applications to be presented later.

The system of nonlinear equations (8) through (12) which defines the discretized problem can be solved using many different types of integration schemes. The implicit one-step Euler backward difference method is employed in this analysis. The time derivative of the temperature is approximated by

$$\frac{\partial\{T\}}{\partial t} \cong \frac{\{T\}_{(i+1)\Delta t} - \{T\}_{(i)\Delta t}}{\Delta t} = \frac{\{\Delta T\}}{\Delta t} \quad , \tag{13}$$

where $\{T\}_{(i)\Delta t}$ is assumed known at time $(i)\Delta t$. In the nonlinear analysis, $\{T\}_{(i+1)\Delta t}$ is calculated using a computational scheme that iterates on the out-of-balance heat flow rate for a given time step. At time $(i+1)\Delta t$, the initial approximation of the increment $\{\Delta T\}^{(0)}$ in nodal point temperatures is calculated by

$$\left(\frac{1}{\Delta t}[C]_{(i)\Delta t} + [K]_{(i)\Delta t}\right)\{\Delta T\}^{(0)} = -[K]_{(i)\Delta t}\{T\}_{(i)\Delta t} - \{\overline{F}\}_{(i+1)\Delta t} - \{\bar{\bar{F}}\}_{(i)\Delta t} \quad . \tag{14}$$

In each iteration, a new temperature increment is computed from

$$\{\Delta T\}^{(P)} = \{\Delta T\}^{(P-1)} + \{\delta T\}^{(P)} \quad , \tag{15}$$

where $\{\delta T\}^{(P)}$ is the $(P)^{th}$ correction to the temperature increment $\{\Delta T\}$. The expression for computing the correction $\{\delta T\}^{(P)}$ is determined by substituting (15) into (13) and using (8) in the form

$$[S]^{(P-1)}_{(i+1)\Delta t}\{\delta T\}^{(P)} = -\left[[K]^{(P-1)}_{(i+1)\Delta t}\{T\}^{(P-1)}_{(i+1)\Delta t} + \frac{1}{\Delta t}[C]^{(P-1)}_{(i+1)\Delta t}\{\Delta T\}^{(P-1)} + \{\overline{F}\}_{(i+1)\Delta t} + \{\bar{\bar{F}}\}^{(P-1)}_{(i+1)\Delta t}\right] \quad , \tag{16}$$

where

$$[S]^{(P-1)}_{(i+1)\Delta t} = \frac{1}{\Delta t}[C]^{(P-1)}_{(i+1)\Delta t} + [K]^{(P-1)}_{(i+1)\Delta t} \tag{17}$$

is evaluated using temperatures

$$\{T\}^{(P-1)}_{(i+1)\Delta t} = \{T\}_{(i)\Delta t} + \{\Delta T\}^{(P-1)} \quad . \tag{18}$$

The iteration continues until convergence is obtained according to the criterion

$$||\{\delta T\}^{(P)}|| \; / \; ||\{T\}^{(P)}_{(i+1)\Delta t}|| < TOL1 \quad , \tag{19}$$

where TOL1 represents an adjustable tolerance.

Equations (14) through (19) constitute the full Newton iterative solution of the governing system of equations (8). To avoid the undesirable computational expense of updating and factorizing the effective stiffness matrix $[S]^{(P-1)}_{(i+1)\Delta t}$ in each iteration, the applications presented in this paper make use of the modified Newton-Raphson scheme. In this method, a new tangent stiffness matrix $[S]_{(n)\Delta t}$ is computed periodically from one of the converged solutions at time $(n)\Delta t$, n=0,1,2,... i, and used in place of $[S]^{(P-1)}_{(i+1)\Delta t}$ in equation (16). Because the matrix $[S]_{(n)\Delta t}$ is held fixed in a given time step, this modified method involves fewer stiffness reformations than full Newton iteration. The frequency of the stiffness updates can be adjusted according to the degree of nonlinearity in the computational model to avoid an excessive number of iterative corrections.

This application of the finite element method to the inverse heat conduction problem considers a two-dimensional model of the (r,θ) cross section of a circular cylinder. An isoparametric [14] discretization is employed, so that the spatial coordinates are interpolated using the same functions N_I as those used for T in equation (6). The N_I associated with the 4- to 8-noded two-dimensional isoparametric element are described in numerous references, including [14] and [15], and will not be given here.

IV. FORMULATION OF THE INVERSE PROBLEM

In this study, the two-dimensional problem of a cylindrical body subjected to a planar surface heat flux $q(\theta,t)$ is considered as depicted in Figure 4. The conditions

$$T(r^p,\theta_\ell,t) = T^p_\ell(t) \qquad 0 \le t \le \hat{t} \quad , \quad \ell = 1,L \tag{20}$$

are prescribed at L equally spaced interior points along a contour of radius r^p near the surface, while the surface heat flux function

$$-k\left(\frac{\partial T}{\partial r}\right)_{r=a} = q(\theta,t) \tag{21}$$

is unknown. The problem is to determine $q(\theta,t)$ and the temperature distribution $T(r,\theta,t)$, $0 \le r \le a$, $0 \le \theta \le 2\pi$, on a specified time domain. Although a circular geometry is assumed here, the basic technique described below for treating the inverse problem is applicable to other geometric shapes with a multiple number of thermocouple sensors judiciously positioned near the surface of the body.

In his treatment of the linear inverse problem, Imber [11] indicates that a successful extrapolation procedure requires the temperature distribution to be known, a priori, throughout a closed region within the body. For a one-dimensional axisymmetric analysis of a cylinder such as that depicted in Figure 1, the temperature can be determined in the closed region $r \le r^p < a$ using data from a single thermocouple sensor positioned at radius r^p. The two-dimensional analog achieved by relaxing the condition of axisymmetry then presumes a time-history of temperature data recorded pointwise on a closed contour of radius r^p, i.e., a "line-source" of temperature data. Because such a volume of measured data

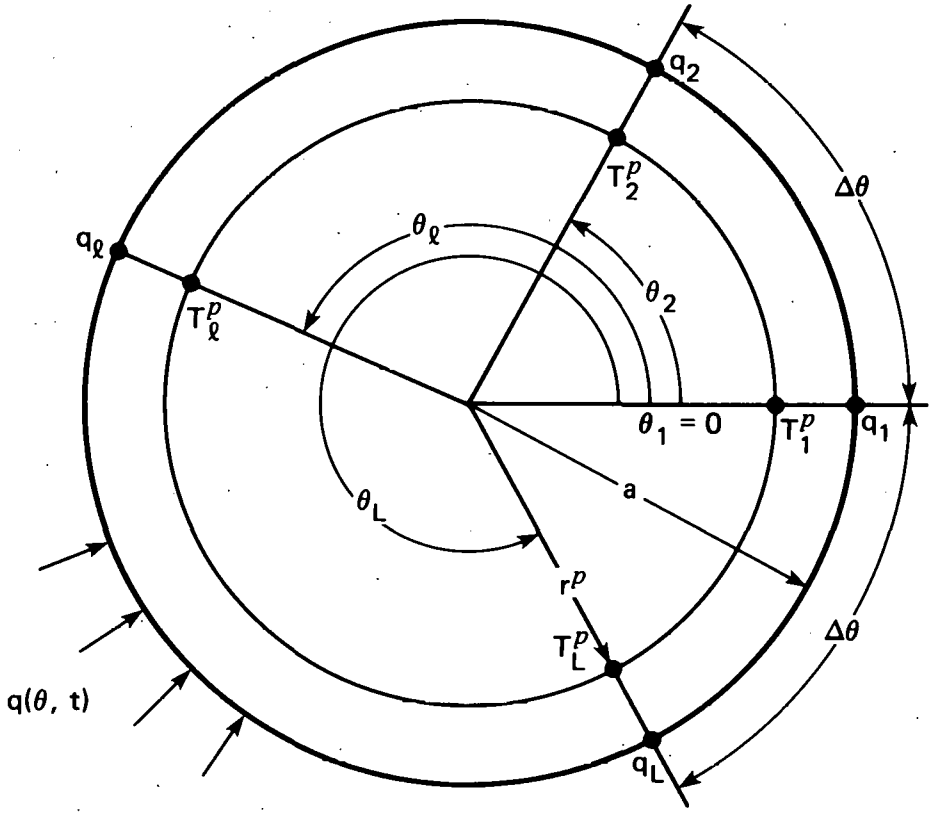

Figure 4. Cross section of heated cylinder

would not be available in any realistic experimental program, the technique described below is based on a limited number of thermocouple sensors discretely positioned on a contour near the surface of the body. Numerical examples presented in the next section illustrate that the accuracy of the technique in approximating the flux boundary condition is improved as the number of temperature sensors per unit arc length on the contour is increased.

The initial step in the development of the method is the discretization of the unknown surface heat flux on the boundary domain using a set of nodal values q_ℓ, $\ell = 1,L$, and suitable interpolating functions R_ℓ (to be specified later), as depicted in Figure 1. Thus, the approximation of the surface heat flux q is given by

$$q(\theta,t) = \sum_{\ell=1}^{L} R_\ell(\theta)\, q_\ell(t) = \{R\}^T \{q\} \quad . \tag{22}$$

One surface flux node is designated for each active thermocouple sensor and positioned at the minimum distance from the sensor node. Numerical tests have indicated that this geometric arrangement produces a stable, well conditioned system of equations for approximating the boundary heat flux function q.

In addition, the nodal values of surface heat flux will be temporally discretized such that in a given time step Δt, $q(\theta,t)$ is represented by

$$q(\theta,t) = \sum_{\ell=1}^{L} R_\ell(\theta)\, q_{\ell;(i)\Delta t}$$

$$= \{R\}^T \{q\}_{(i)\Delta t} \qquad (i-1)\Delta t < t \leq (i)\Delta t \quad i \geq 1 \quad . \tag{23}$$

For a given $i \geq 1$, it is assumed that $\{q\}_{(1)\Delta t}$, $\{q\}_{(2)\Delta t}$, ..., $\{q\}_{(i)\Delta t}$ are known. To determine $\{q\}_{(i+1)\Delta t}$, an analysis interval of $J \geq 1$ time steps is selected, as depicted in Figure 5.[1] In the next step, $\{q\}$ is estimated over the analysis interval $(i)\Delta t < t \leq (i+J)\Delta t$ using relations that take the trend of q into account. For the first time step in the interval,

$$\{q\}_{(i+1)\Delta t} = \{q\}_{(i)\Delta t} + (\{q\}_{(i)\Delta t} - \{q\}_{(i-1)\Delta t}) \tag{24}$$

and for the "future" time steps

$$\{q\}_{(i+j)\Delta t} = \{q\}_{(i+j-1)\Delta t} + \beta \cdot (\{q\}_{(i+j-1)\Delta t} - \{q\}_{(i+j-2)\Delta t}) \tag{25}$$

for $2 \leq j \leq J$, where $0 \leq \beta \leq 1$ is an adjustable parameter.[2] Thus, the interpolated boundary conditions can be estimated for each time step in the analysis interval according to the relation

$$q(\theta)_{(i+j)\Delta t} = \{R\}^T \{q\}_{(i+j)\Delta t} \qquad 1 \leq j \leq J \quad . \tag{26}$$

Then the boundary value problem (equations (1) through (5)) cast in the discretized finite element formulation (equations (8) through (12)) is solved over the analysis interval $(i)\Delta t < t \leq (i+J)\Delta t$ using conditions (24) - (26) in the surface integral of equation (11).

The objective of the method is to select $\{q\}_{(i+1)\Delta t}$ to achieve the closest agreement in a least squares sense between the computed and input thermocouple temperatures over the analysis interval. This is

---

[1] For elementary one-dimensional models with characteristic dimension a, Beck [7] recommends values of J that are appropriate for given values of the dimensionless time step $\Delta\tau = \alpha\Delta t/a^2$.

[2] $\{q\}_0$ is determined from conditions at the initial time.

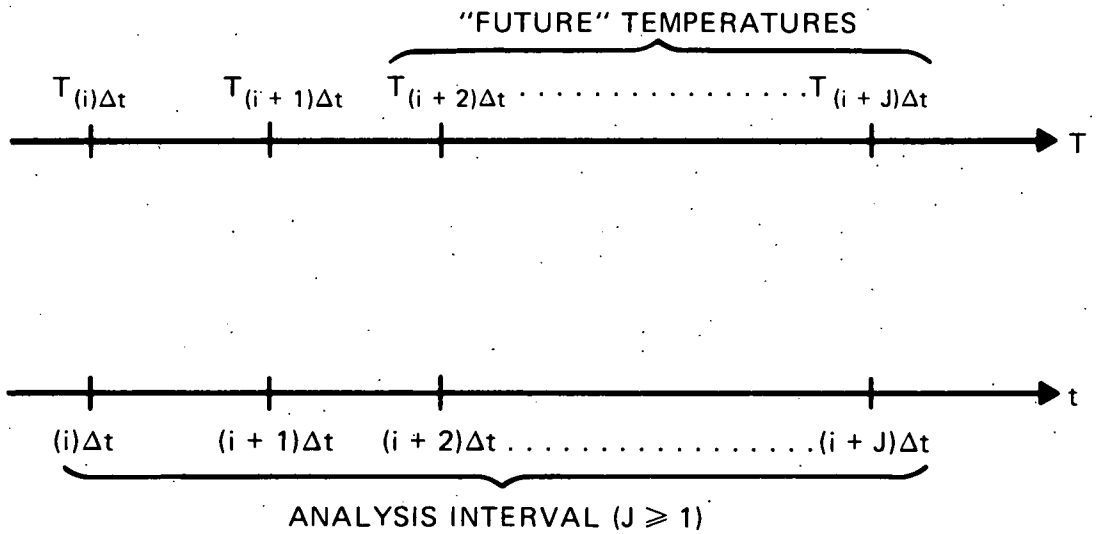

Figure 5. Analysis interval for computing surface heat flux q

accomplished by minimizing the weighted sum of squares function

$$f(\{q\}_{(i+1)\Delta t}) = \sum_{j=1}^{J} w_j \sum_{\ell=1}^{L} \left(T_{\ell;(i+j)\Delta t} - T^p_{\ell;(i+j)\Delta t}\right)^2$$

$$= \sum_{j=1}^{J} w_j \{T - T^p\}^T_{(i+j)\Delta t} \{T - T^p\}_{(i+j)\Delta t} \qquad (27)$$

with respect to the L nodal parameters represented by the array $\{q\}_{(i+1)\Delta t}$. In equation (27), $\{T\}$ and $\{T^p\}$ are the computed and input temperatures at the interior thermocouple locations (r^p,θ_ℓ), $\ell = 1,L$. The weighting functions defined by $w_j = j^2$ were suggested by Muzzy et al. [9] in a one-dimensional finite difference application of Beck's method.[3]

The minimization procedure for the function f of (27) is based on an iterative technique that is a generalization of Beck's one-dimensional formulation. For the $(H)^{th}$ iterative correction $\{\Delta q\}^{(H)}$ to the minimizing nodal parameters $\{q\}_{(i+1)\Delta t}$, the elements of the temperature array $\{T\}^{(H)}_{(i+j)\Delta t}$ in (27) are approximated by a truncated Taylor series expansion

$$T^{(H)}_{\ell;(i+j)\Delta t} \simeq T^{(H-1)}_{\ell;(i+j)\Delta t} + \sum_{k=1}^{L} \frac{\partial T^{(H-1)}_{\ell;(i+j)\Delta t}}{\partial q^{(H)}_{k;(i+1)\Delta t}} \Delta q^{(H)}_k \quad , \quad \ell = 1,L \qquad (28)$$

where

$$\Delta q^{(H)}_k = q^{(H)}_{k;(i+1)\Delta t} - q^{(H-1)}_{k;(i+1)\Delta t} \qquad k = 1,L \quad . \qquad (29)$$

If the heat conduction model is linear, this expression is exact and no iteration is required. The partial derivatives in (28), referred to as

[3] Beck's one-dimensional formulation uses $w_j = 1$ for all j.

sensitivity coefficients, are approximated numerically according to the expression

$$ {}_{j}\phi_{\ell k}^{(H-1)} = \frac{\partial T_{\ell;(i+j)\Delta t}^{(H-1)}}{\partial q_{k;(i+1)\Delta t}^{(H)}} \qquad \ell,k = 1,L \quad j = 1,J $$

$$ \approx \frac{T_{\ell;(i+j)\Delta t}\left(\{q^*\}_{(i+1)\Delta t}^{(H-1)}\right) - T_{\ell;(i+j)\Delta t}\left(\{q\}_{(i+1)\Delta t}^{(H-1)}\right)}{\lambda q_{k;(i+1)\Delta t}^{(H-1)}} \quad , \qquad (30) $$

where $\{q^*\}$ is obtained from $\{q\}$ by perturbing the k^{th} component, i.e., $q_k^* = (1+\lambda)q_k$ and $q_m^* = q_m$, $m \neq k$. A value of $\lambda = 1 \times 10^{-3}$ is used in the present study.

In each iterative correction to $\{q\}_{(i+1)\Delta t}$, (J)(1+L) conventional solutions of the finite element heat conduction model (equations (8) - (12)) are required to compute the array (30) of sensitivity coefficients. With the ϕ's thus determined, the extremizing condition

$$ \frac{\partial f}{\partial \{q\}_{(i+1)\Delta t}} = \underline{0} \qquad (31) $$

is used to compute the incremental correction. When (28) is substituted into (27) and the differentiation (31) is performed, the $(H)^{th}$ correction $\{\Delta q\}^{(H)}$ is determined from the expression

$$ [A]^{(H-1)} \{\Delta q\}^{(H)} = \{D\}^{(H-1)} \quad , \qquad (32) $$

where the components are given by

$$ A_{\ell k}^{(H-1)} = \sum_{j=1}^{J} w_j \sum_{m=1}^{L} {}_{j}\phi_{m\ell}^{(H-1)} \, {}_{j}\phi_{mk}^{(H-1)} \quad , \qquad (33) $$

$$ D_{\ell}^{(H-1)} = \sum_{j=1}^{J} w_j \sum_{k=1}^{L} \left(T_{k;(i+j)\Delta t}^{p} - T_{k;(i+j)\Delta t}^{(H-1)}\right) {}_{j}\phi_{k\ell}^{(H-1)} \quad . \qquad (34) $$

The correction (32) is then used to update the nodal array $\{q\}^{(H-1)}_{(i+1)\Delta t}$ of surface flux according to equation (29). Generally, the iteration is continued until convergence is achieved according to the criterion

$$||\{\Delta q\}^{(H)}|| \; / \; ||\{q\}^{(H)}_{(i+1)\Delta t}|| < TOL2 \tag{35}$$

for some prescribed tolerance TOL2 > 0.

The discretized approximation of the surface heat flux

$$q(\theta)_{(i+1)\Delta t} = \{R\}^T \{q\}_{(i+1)\Delta t} \tag{36}$$

thus determined provides a conventional boundary condition (for equation (11)) in the next single time step Δt only. The analysis interval is then shifted by one time step and the process is repeated.

In the numerical applications of this technique in the next section, the surface flux interpolating functions $\{R\}$ have the form

$$R_\ell(\theta) = \begin{cases} \cos^2\left[\frac{\pi}{2} \; \frac{(\theta - \theta_\ell)}{\Delta\theta}\right] & \theta_\ell - \Delta\theta \leq \theta \leq \theta_\ell + \Delta\theta \\ 0 & \text{otherwise} \end{cases} \tag{37}$$

for $\ell = 1,L$. The functions (37) depicted in Figure 6 have the properties

$$R_\ell(\theta_k) = \begin{cases} 1 & \ell = k \\ 0 & \ell \neq k \end{cases} \qquad \ell,k = 1,L \tag{38}$$

$$R_\ell(\theta) + R_{\ell+1}(\theta) = 1 \qquad \theta_\ell \leq \theta \leq \theta_{\ell+1}$$
$$(R_{L+1} \equiv R_1 \;\; , \;\; \theta_{L+1} \equiv \theta_1) \quad . \tag{39}$$

It follows from equation (39) that the interpolation (22) can represent a uniform surface heat flux.

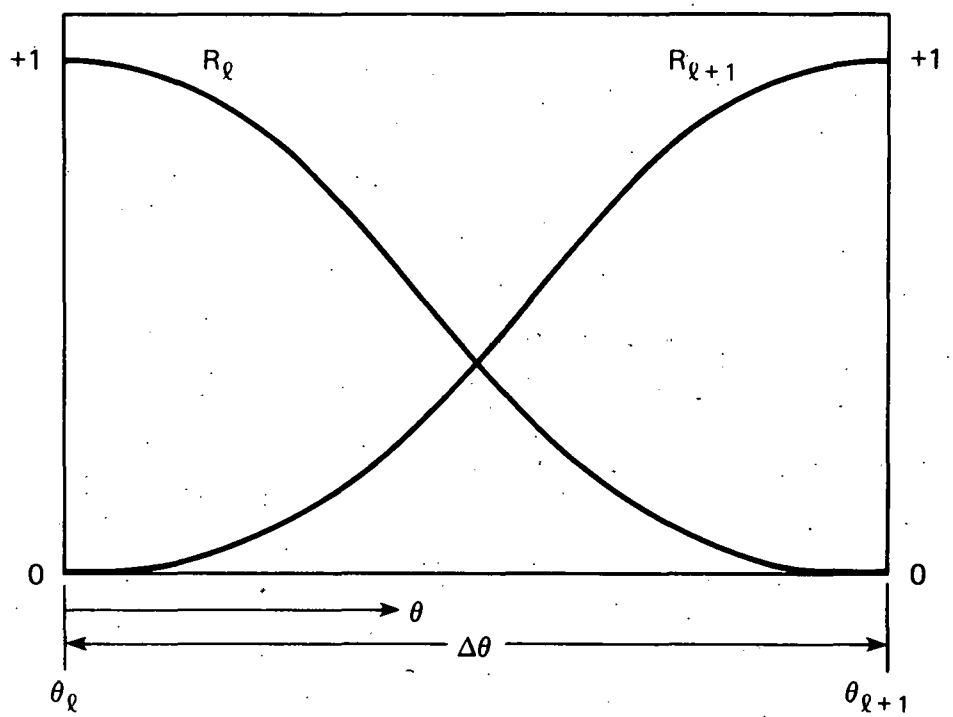

Figure 6. Interpolating functions for surface heat flux

V. NUMERICAL APPLICATIONS

The two-dimensional inverse formulation developed in the preceding sections has been implemented in the digital computer program ORMDIN, as described in Appendices A and B of this report. Program ORMDIN is applied here to a composite rod containing an electric heating element and thermocouple sensors. This heater rod represents one member of a rod array (THTF bundle 3) that is designed for test purposes to simulate a nuclear fuel bundle. The heater rod bundle is positioned in a thermal-hydraulics test loop that is used to study hypothetical loss-of-coolant accidents in pressurized-water nuclear reactors [1].[4]

A heater rod cross section and the corresponding two-dimensional finite element discretization used in the inverse analysis are depicted in Figures 4 and 5. The rod has a nominal heated length of 366 cm (144 in.) and is constructed with a stainless steel outer sheath. Attached to the inner surface of this sheath at equal intervals are twelve chromel-alumel thermocouple assemblies, 0.05 cm (0.02 in.) in diameter. Four additional sensors are positioned in the center of the rod. Only four of the sixteen thermocouples actively record data in the cross section of Figure 7, namely the three boron nitride- (BN) filled thermocouples attached to the outer sheath and one of the center rod thermocouples; the junctions of the remaining thermocouples are positioned in different axial planes of the rod. Boron nitride is used as a filler and an insulator between the inconel heating element and the thermocouple assemblies. In the finite element model of the heater rod

[4]This test facility is operated by the Oak Ridge National Laboratory (ORNL) Pressurized-Water Reactor Blowdown Heat Transfer Separate-Effects Program, which is part of the overall light-water reactor safety research program of the Nuclear Regulatory Commission.

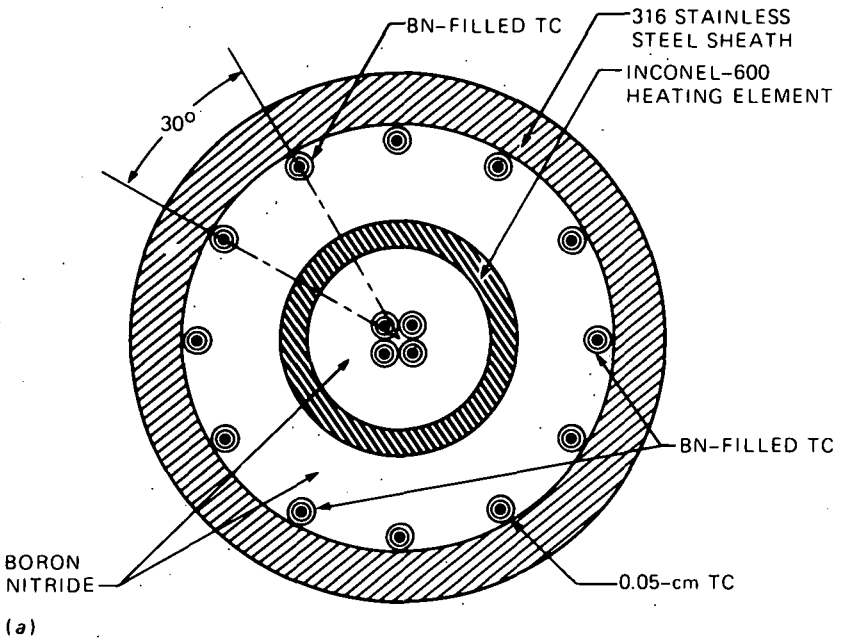

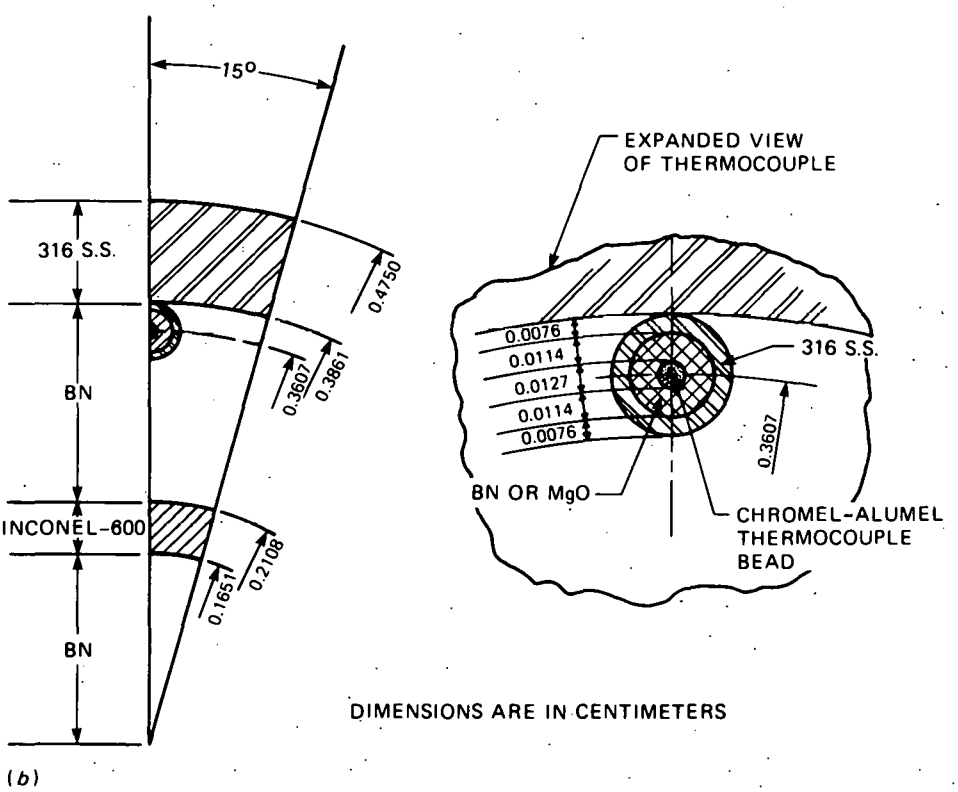

Figure 7. Electrically heated rod with interior thermocouple sensors (THTF bundle 3 FPS)
(a) cross section
(b) dimensions

(Figure 8), each thermocouple at the outer sheath is modeled with two quadrilateral elements that are assigned the appropriate material properties of BN or MgO and the same total cross sectional area as the *in situ* circular sheaths. Those in the center of the rod are not used to drive the inverse computation and are not included in the finite element discretization.

The thermophysical properties of thermal conductivity k and specific heat c are temperature dependent for each material in the rod. Except for the thermal conductivities of MgO and BN, these properties are determined for each material as a function of temperature from an optimum polynomial fit to available data, as given in Reference [2]. The thermal conductivities for the MgO and BN depend on packing density and must be determined *in situ* as part of the rod calibration procedure [16] prior to each test.

The first numerical example[5] was selected to evaluate the performance of the technique in solving the inverse problem for the finite element model of Figure 8. A standard initial-boundary value solution was obtained from the finite element formulation (8) - (12) using the prescribed surface heat flux function

$$q(\theta,t) = 47.31 + 126.2[\sin(\tfrac{1}{2}\{\theta - 2\pi t\})]^{2+12t} \text{ watts/cm}^2 \quad ,$$

$$0 \leq t \leq 1.0 \tag{40}$$

a constant heat generation rate $Q = 5274$ watts/cm^3, a time step $\Delta t = .01$ secs, and initial center rod temperature $T_{center} = 441.2°C$. From this direct solution, the temperature transients of Figure 9 were calculated

[5]The inverse calculations presented in this section were performed using TOL1 = .001, equation (19); $\beta = 0.5$, equation (25); TOL2 = 0.05, equation (35).

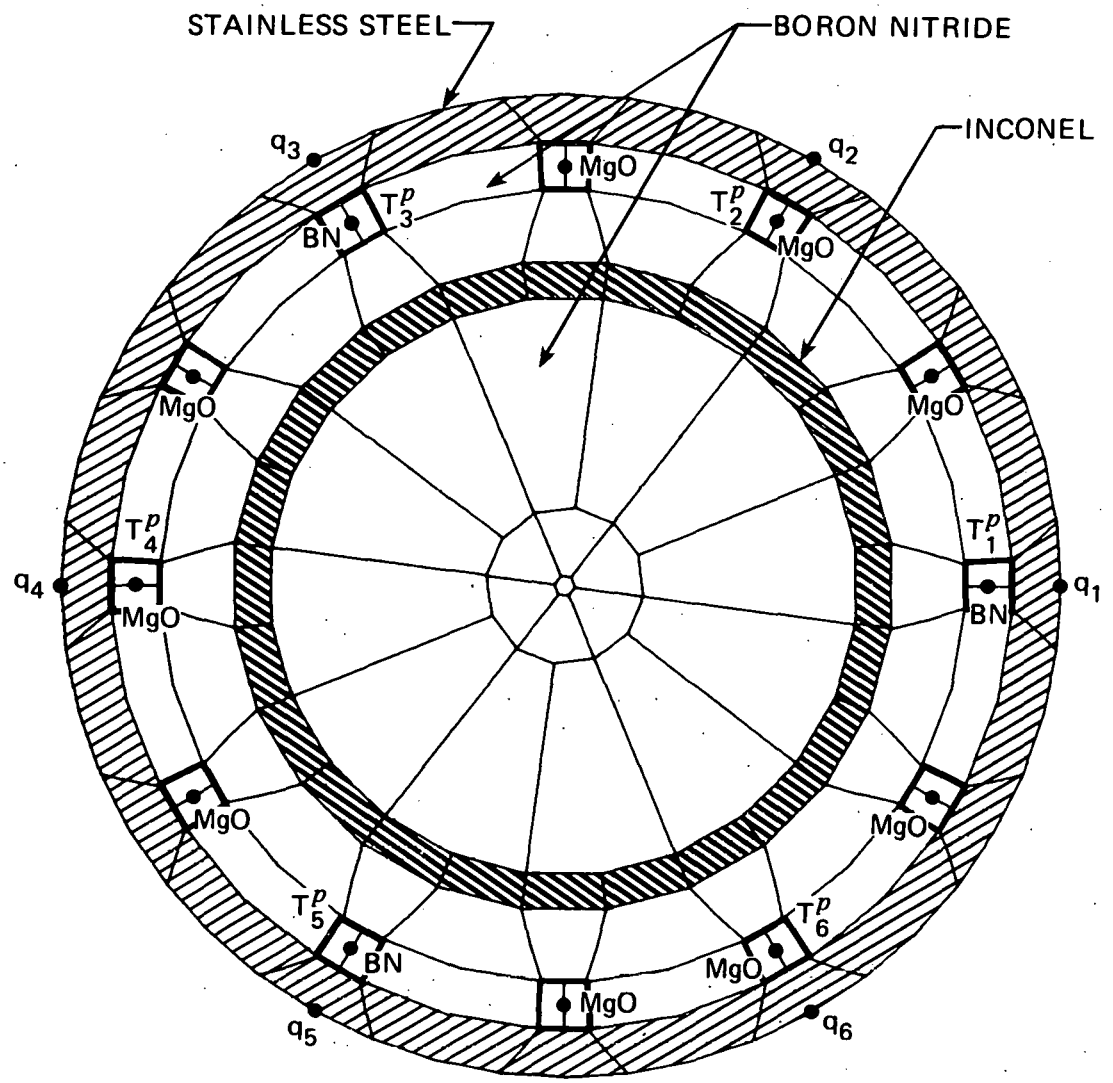

Figure 8. Two-dimensional finite element model of heater rod cross section (THTF bundle 3 FPS): 126 elements; 288 nodes

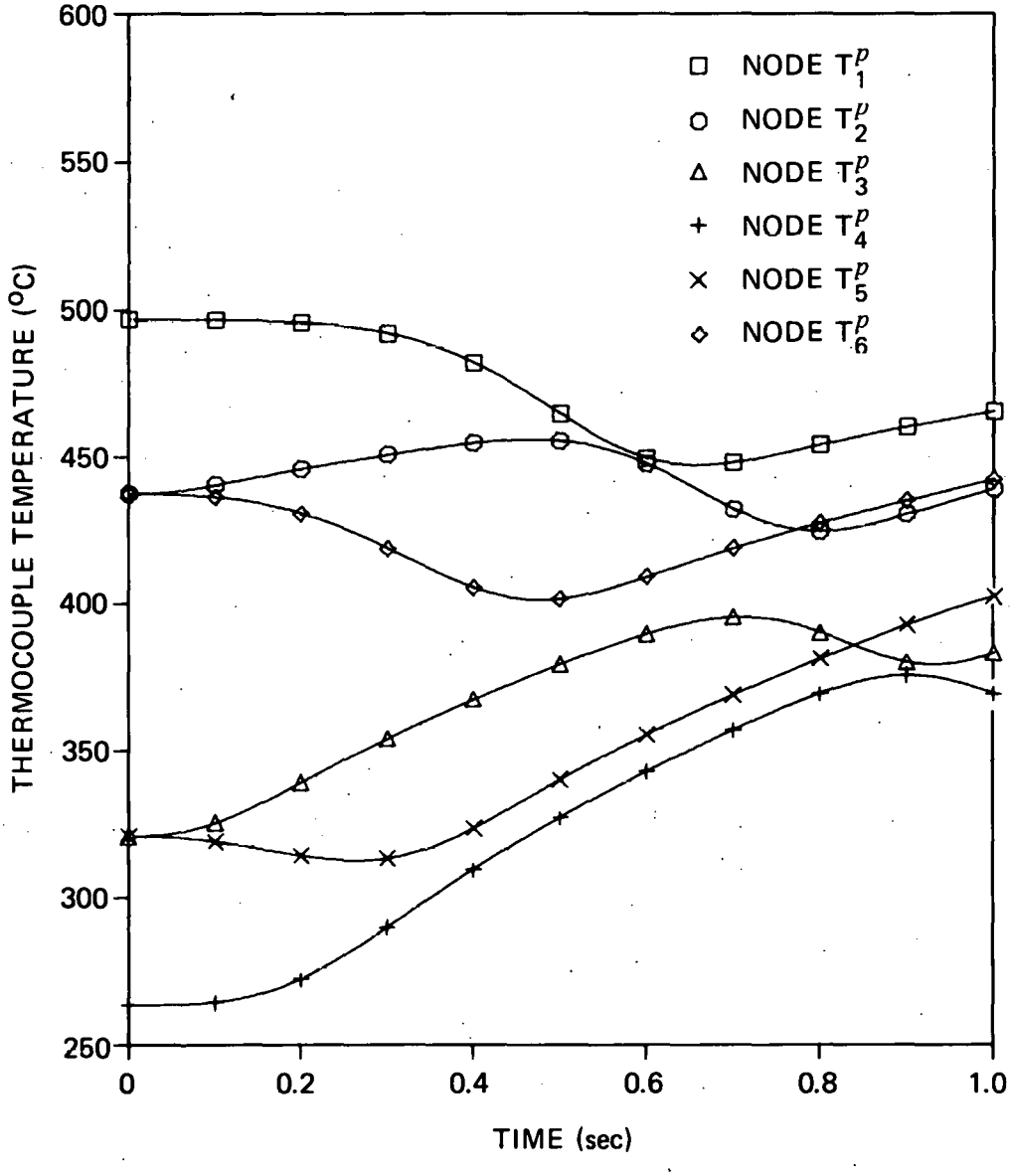

Figure 9. Test case: Calculated temperatures at thermocouple locations from direct solution

at the thermocouple locations 1 through 6 of the discrete model (Figure 8). With the thermocouple transients of Figure 9 serving as input, two different inverse analyses were performed in an attempt to reproduce the surface flux boundary condition (40). The first analysis utilized input data from only three of the thermocouples (L = 3), those numbered 1, 3, and 5 in Figure 8, while the second utilized data from six thermocouples (L = 6). The analysis interval consisted of only one time step (J = 1). Results from the two inverse analyses are compared with the known direct solution in Figures 10 and 11 at different times. Throughout the transient, the inverse analysis using six active thermocouples consistently produced a good approximation of both the surface flux function (40) and the surface temperatures. As illustrated in Figure 10, the solution using three active thermocouples was not as successful in approximating the surface variables at those times when the localized perturbation in the surface flux was not "near" an active sensor. This example demonstrates that, within practical limits, the prediction of surface conditions is improved as the number of thermocouple sensors per unit length of contour is increased.

In the second numerical example, the inverse formulation is applied to actual thermocouple transients taken from a representative test of ORNL's single-rod test apparatus.[6] The heater power input to the rod during the period of the transient considered here is essentially constant at $Q = 5300$ watts/cm^3. Figure 12 illustrates the time-history of the thermocouple temperatures recorded by the active BN-filled

[6]The single-rod test facility [1] at ORNL is used primarily to qualify heaters for the large rod bundle loop and to obtain blowdown heat transfer results for a single rod in an annular geometry. The test data utilized in this example were recorded during blowdown FCTF 79-1-6 at axial level D in the heater rod.

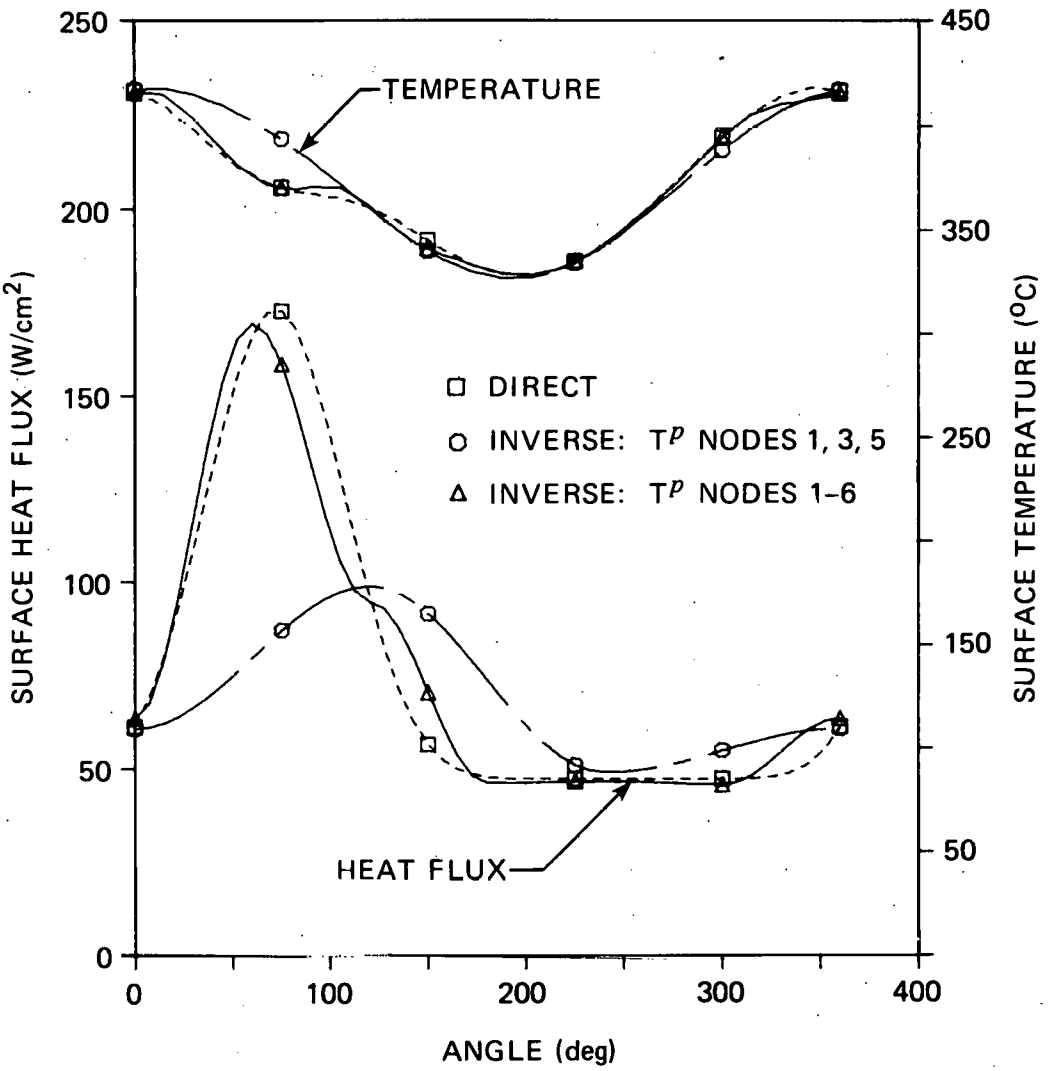

Figure 10. Test case: Comparison of direct solution with inverse solutions at time 0.7 sec

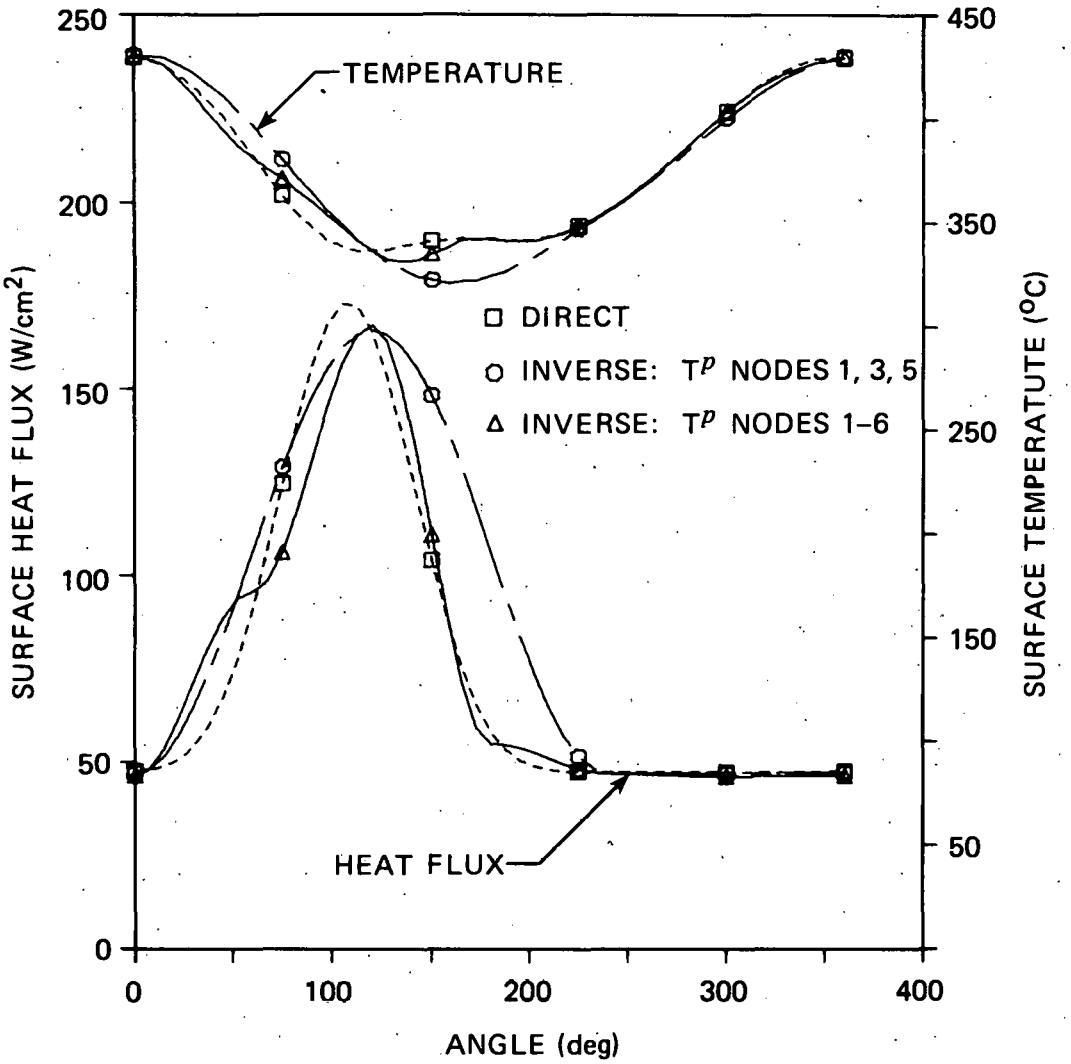

Figure 11. Test case: Comparison of direct solution with inverse solutions at time 0.8 sec

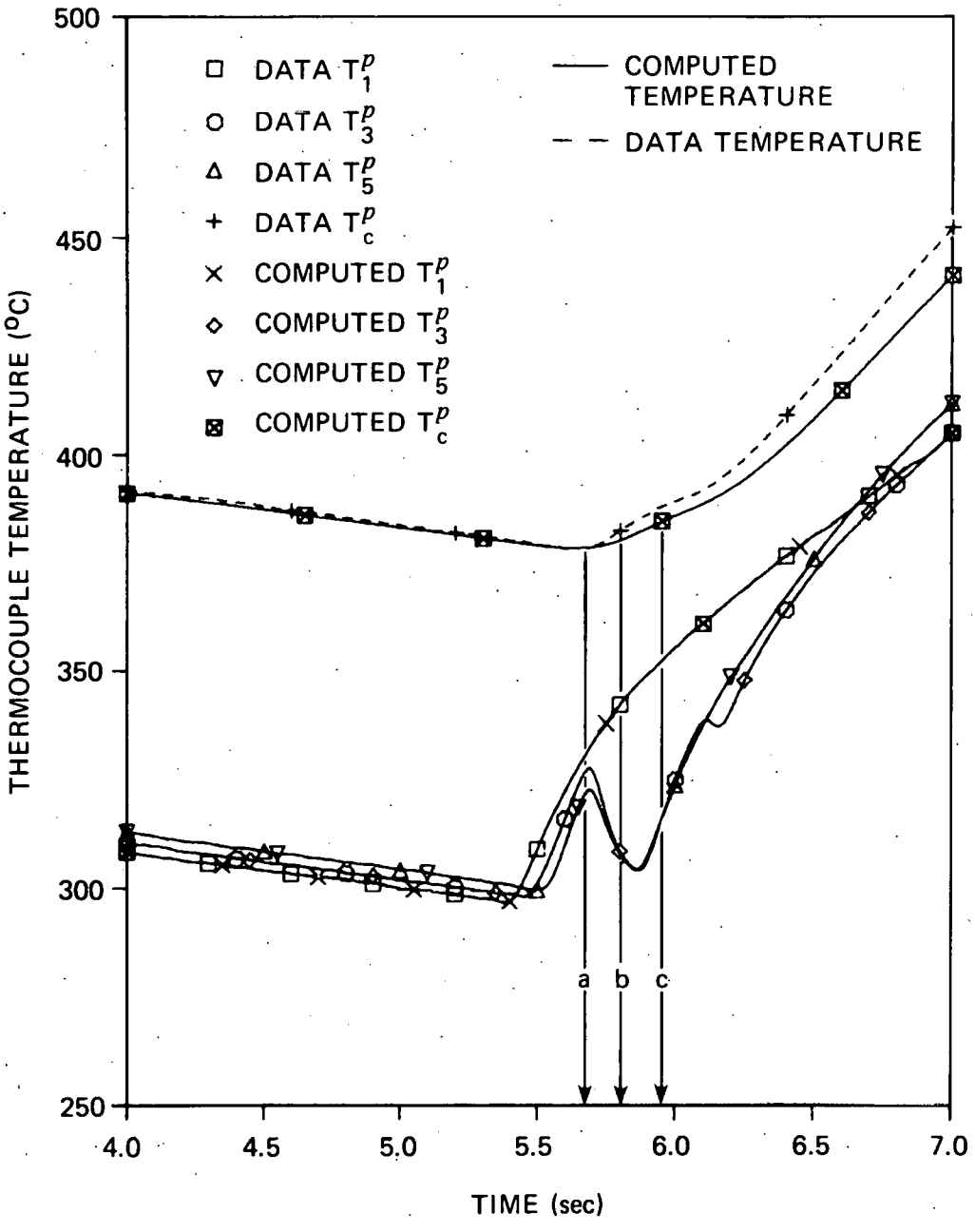

Figure 12. Experimental case: Comparison of inverse solution (Δt=0.01 and J=2) with measured temperature data

sensors (1, 3, and 5 in Figure 8) and by the one active center thermocouple. The acquisition interval for these data is $\Delta t = 0.01$ secs. In the same figure, the temperatures computed at the BN thermocouple locations in an inverse solution (for $\Delta t = 0.01$ secs and $J = 2$) are compared with the input data; the error is not discernible on the scale of these plots. Because the center thermocouple data are not used in the inverse computation, comparison of these data with the computed center rod temperatures permits an evaluation of the rod finite element model. This comparison can be only approximate due to uncertainty in the precise orientation of the center thermocouple assembly and to the absence of appropriate material modeling of the assembly in the discretization. Agreement between the measured and computed values is generally good, although a slight divergence appears at time $t \approx 5.75$ secs when gradients and time rates of temperature become pronounced in the center of the rod.

Figures 13 - 15 illustrate the computed time history of surface conditions at node q_3 in Figure 8 for a time step $\Delta t = 0.01$ secs and three different analysis intervals. The results for one time step in the analysis interval, $J = 1$ (Figure 13), indicate that the measured data of Figure 6 require the use of future temperatures to reduce oscillations in the computed values. The solution using two time steps, $J = 2$ (Figure 14), removes much of the "noise" from the flux time history without severe rounding of rapid changes that begin at time $t \approx 5.5$ secs. The results for $J = 3$ (Figure 15) lead to additional smoothing of the solution and illustrate the tendency to "round off" rapid changes as J is increased. For the finite element model of Figure 8 and a selected time step of $\Delta t = .01$ secs, the use of one future temperature appears optimal for

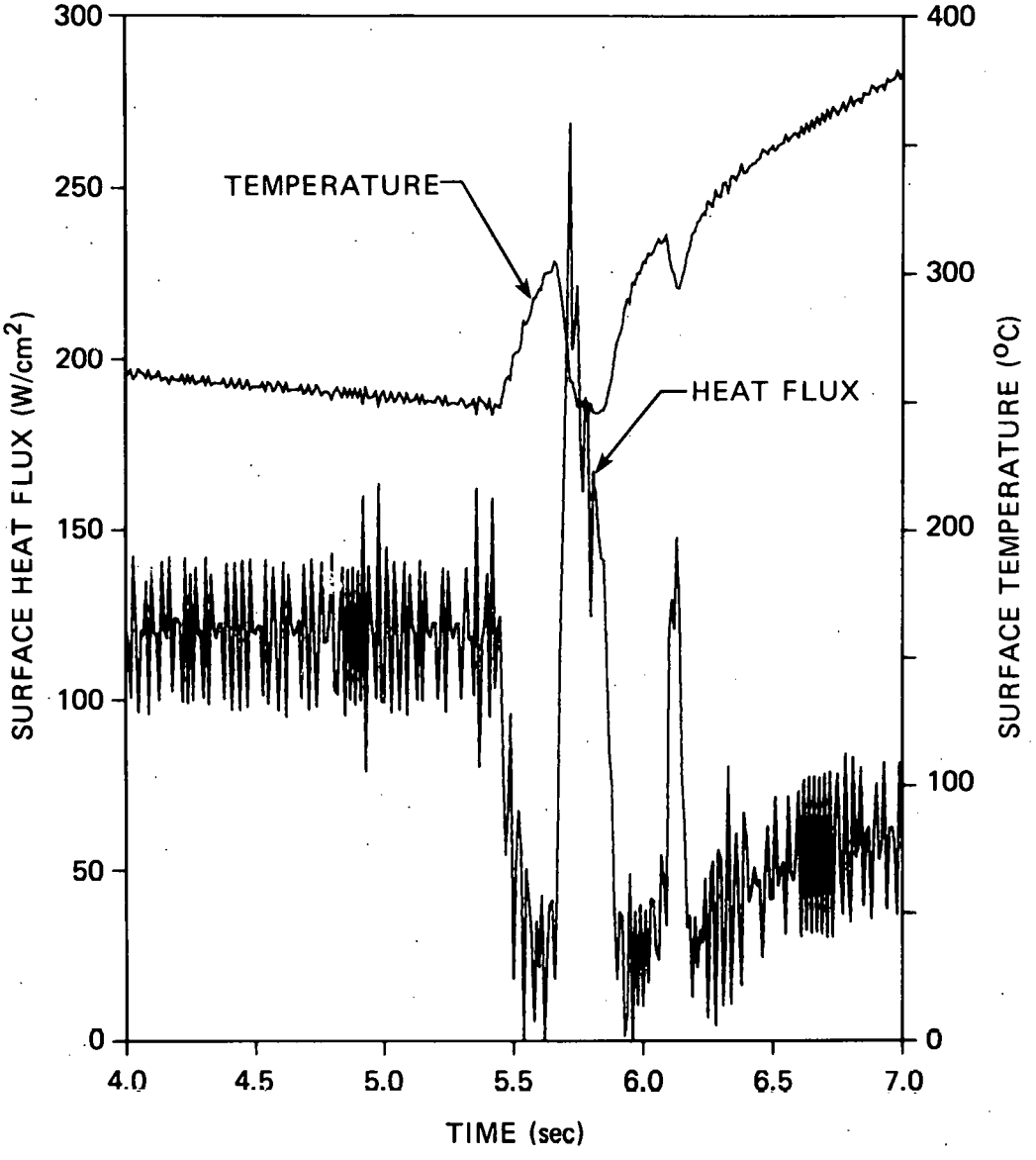

Figure 13. Experimental case: Inverse solution at surface node q_3 using one time step in analysis interval (J=1)

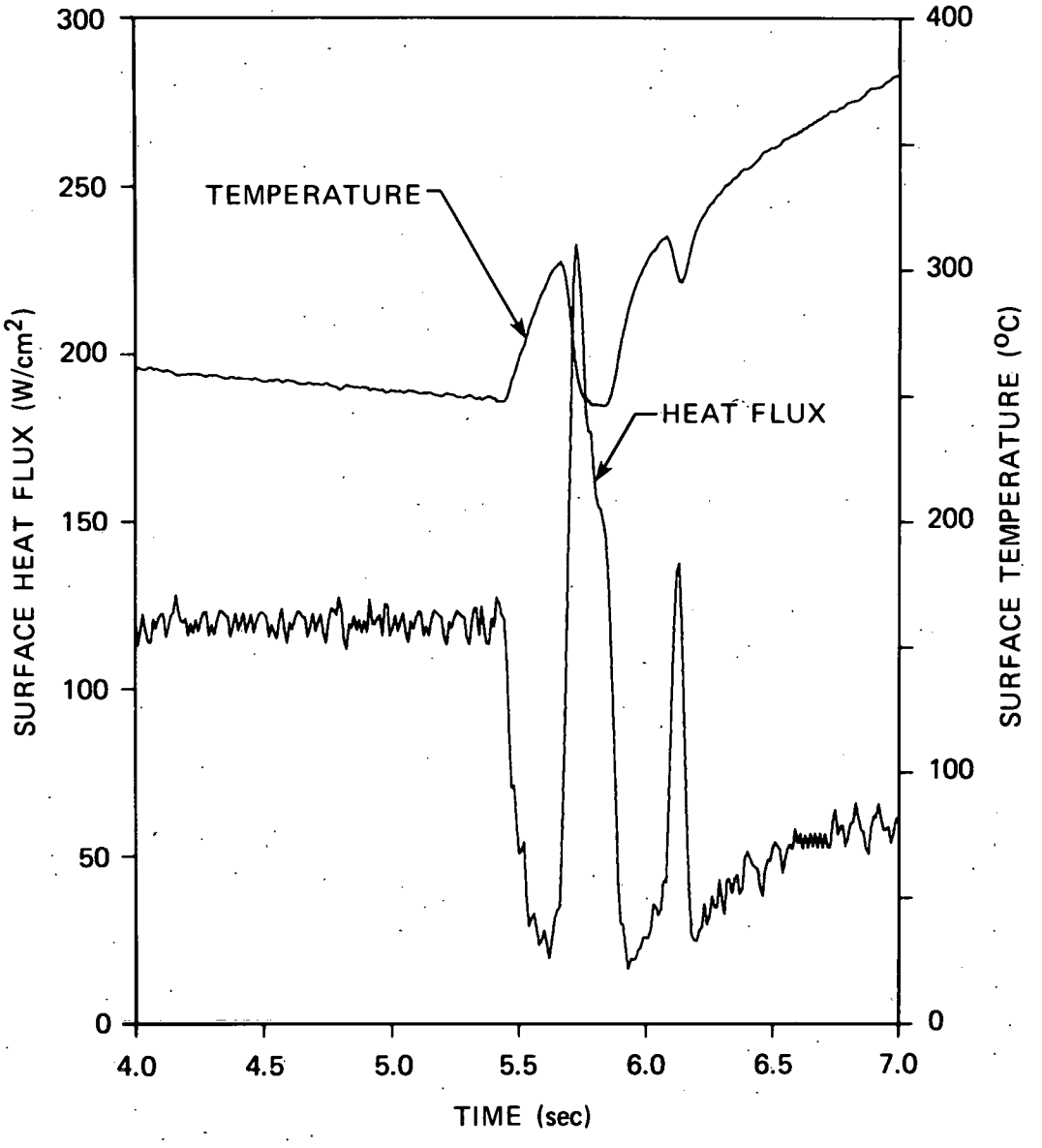

Figure 14. Experimental case: Inverse solution at surface node q_3 using two time steps in analysis interval (J=2)

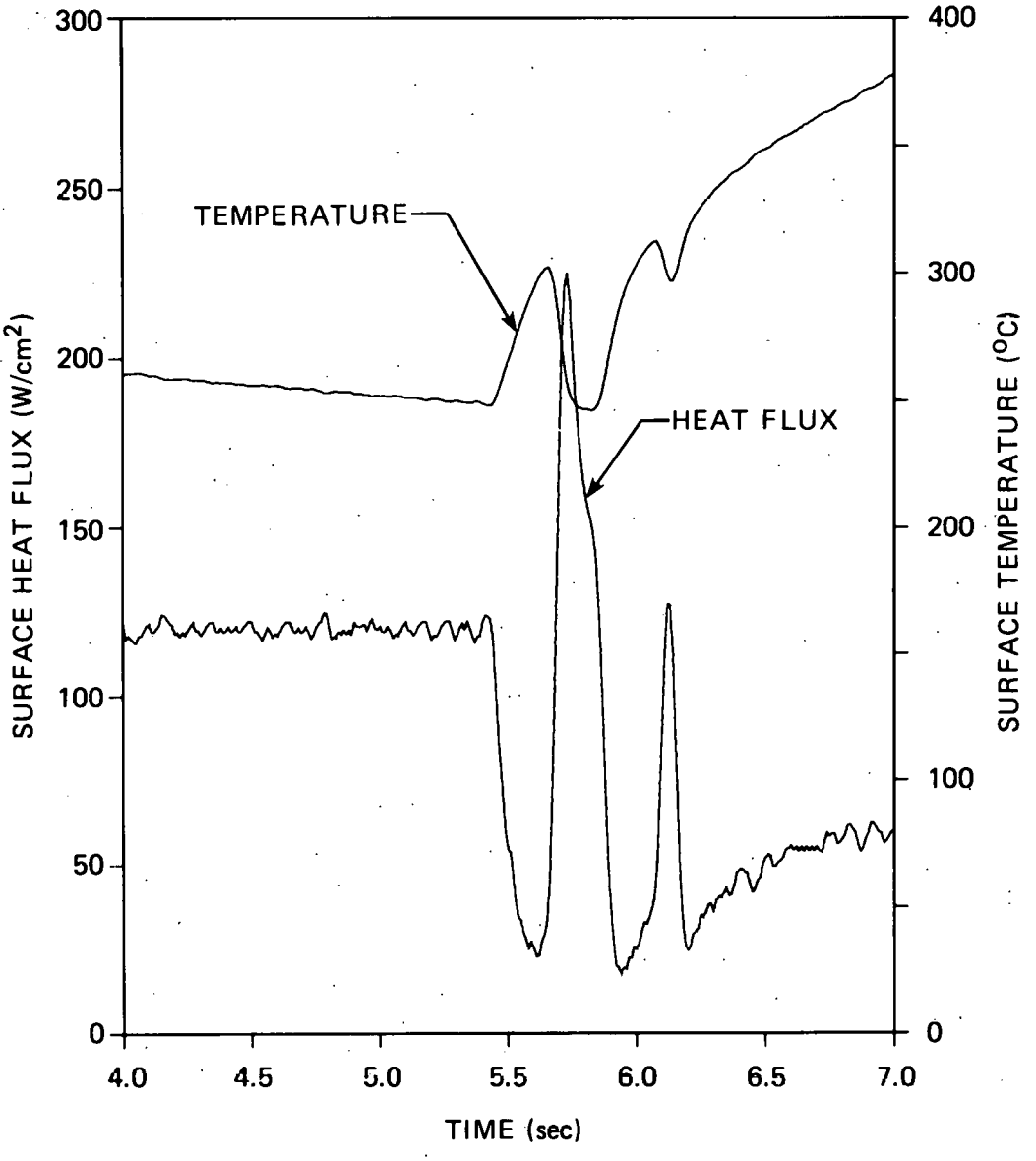

Figure 15. Experimental case: Inverse solution at surface node q_3 using three time steps in analysis interval (J=3)

reducing oscillations. Figure 16 compares the surface conditions at time t = 5.85 secs for the above three solutions.

In the experimental apparatus that produced the thermocouple transients of Figure 12, the heater rod surface is exposed to a transient two-phase flow that is primarily parallel to the rod axis. At point (a) in Figure 12 (time t = 5.65 secs), the entire surface of the rod cross section has departed from nucleate boiling; at point (b) (time t = 5.80 secs), part of the surface experiences a "rewet" with an accompanying drop in temperature; at (c) (time t = 5.95 secs) the entire surface is in transition to film boiling. Contour plots in Figure 17 illustrate the change in temperature distribution for the cross section of the rod during this portion of the transient.

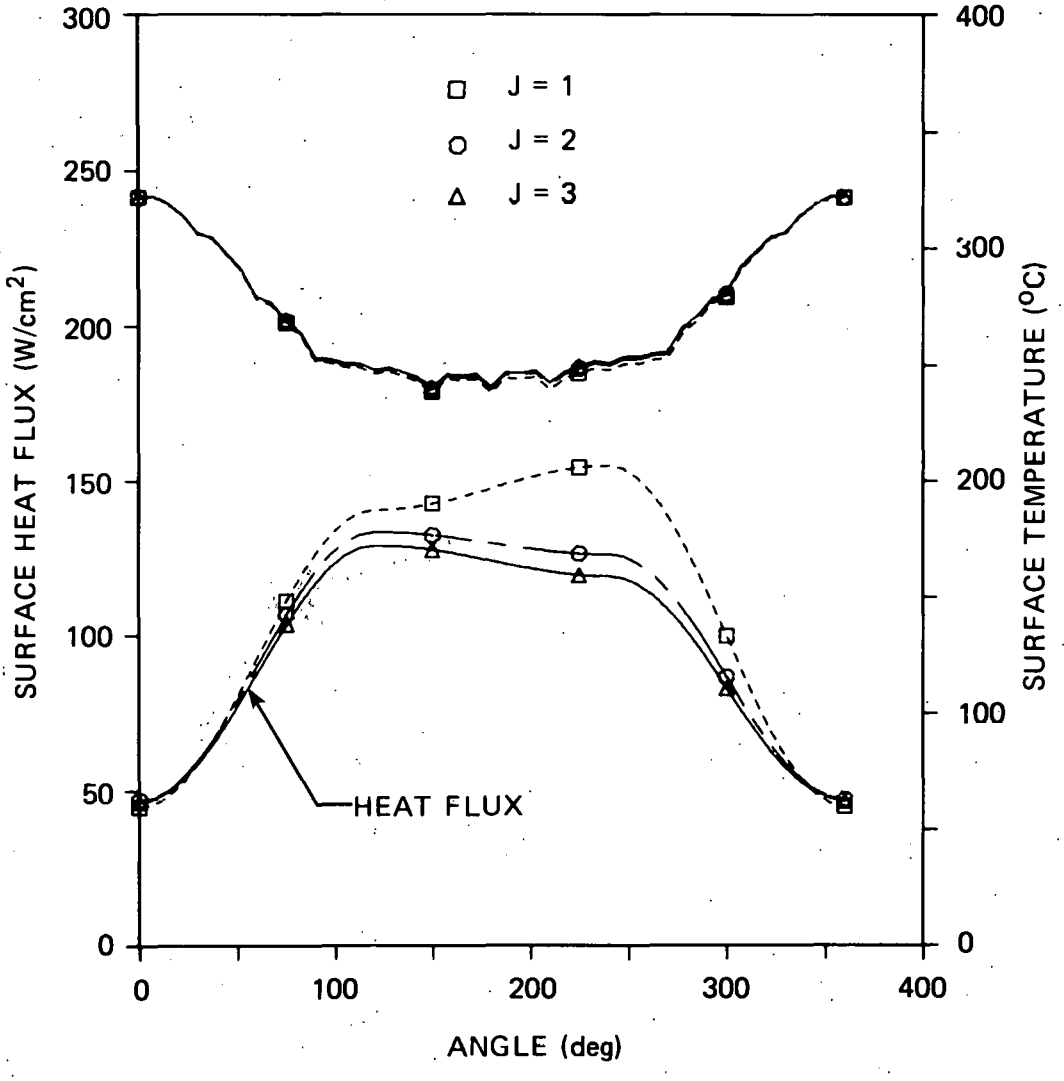

Figure 16. Experimental case: Surface conditions at time 5.85 sec

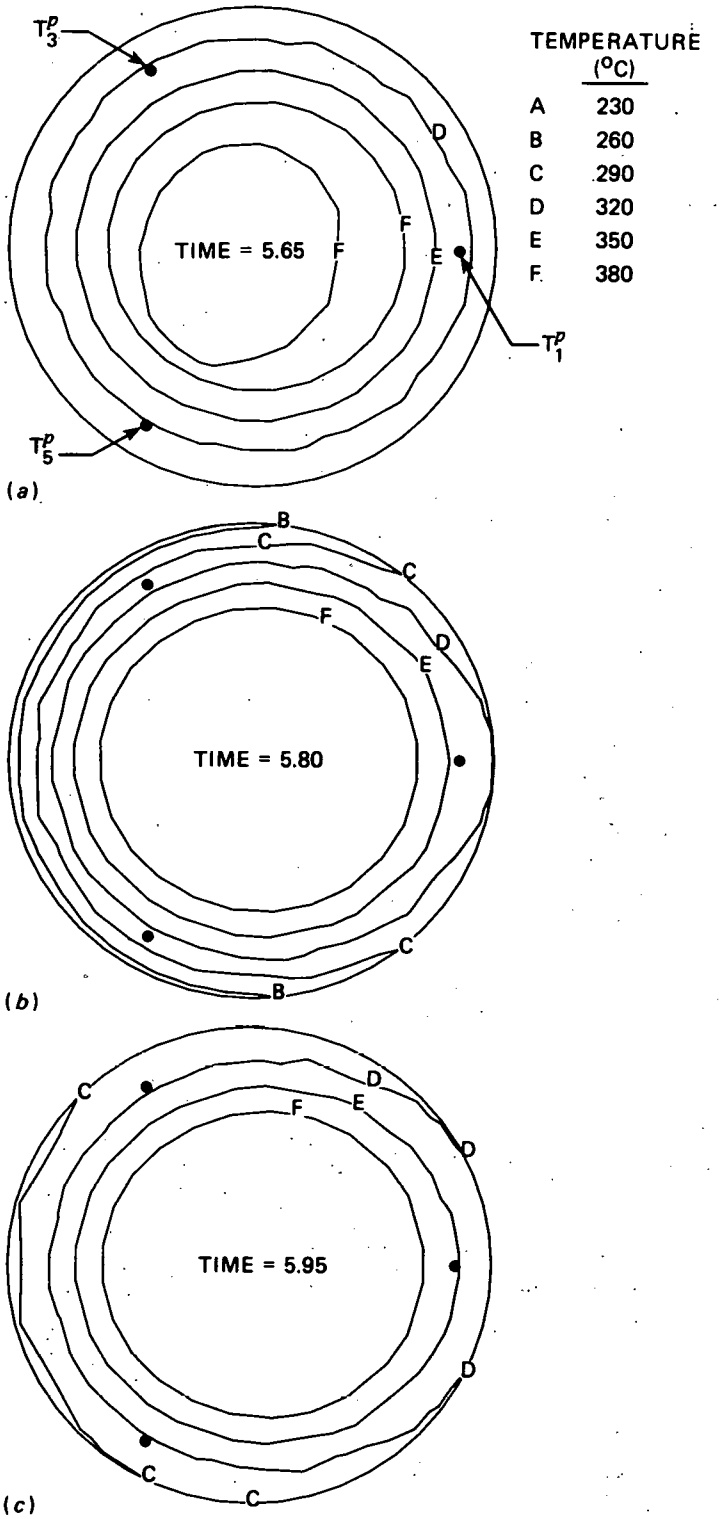

Figure 17. Experimental case: Temperature contours (deg C)
(a) time 5.65 sec
(b) time 5.80 sec
(c) time 5.95 sec

VI. SUMMARY AND CONCLUDING REMARKS

This report has presented a two-dimensional formulation of the inverse heat conduction problem that is applicable to composite bodies with temperature-dependent thermophysical properties. The formulation, based on a finite element heat conduction model and a generalization of Beck's one-dimensional nonlinear estimation procedure, was implemented in the digital computer program ORMDIN. Applications of program ORMDIN to an electrically heated composite rod were examined in the study. In the first example, a conventional initial-boundary value solution, with a known surface heat flux, was used as input for the inverse calculation. The computed surface heat flux was compared with the imposed heat flux for two different thermocouple configurations. These comparisons indicate that, within practical limits, the approximation of surface conditions is improved as the number of thermocouple sensors per unit length of contour is increased. Finally, the technique was applied to experimentally determined temperature transients recorded at thermocouple sensors in the interior of the rod. The results presented here demonstrate that the inverse formulation is capable of successfully treating experimental data. Consideration of future temperatures in calculating surface conditions permits the use of small time steps while avoiding severe oscillations or numerical instabilities due to errors in measured data.

REFERENCES

1. "Project Description, ORNL-PWR Blowdown Heat Transfer Separate-Effects Program — Thermal Hydraulic Test Facility (THTF)," ORNL/NUREG/TM-2, February 1976.

2. Ott, L. J. and R. A. Hedrick, "ORINC — A One-Dimensional Implicit Approach to the Inverse Heat Conduction Problem," ORNL/NUREG-23, November 1977.

3. Bass, B. R., "INCAP: A Finite Element Program for One-Dimensional Nonlinear Inverse Heat Conduction Analysis," NUREG/CR-0832, ORNL/NUREG/CSD/TM-8, July 1979.

4. Ott, L. J. and K. W. Childs, "Surface Heat Flux Perturbations in BDHT Fuel Pin Simulators," NUREG/CR-0610, ORNL/NUREG-54, April 1979.

5. Turner, W. D., D. C. Elrod, and I. I. Siman-Tov, "HEATING5 — An IBM 360 Heat Conduction Program," ORNL/CSD/TM-15, March 1977.

6. Imber, M., "Nonlinear Heat Transfer in Planar Solids: Direct and Inverse Applications," AIAA Journal, Vol. 17, No. 2, February 1979, pp. 204-212.

7. Beck, J. V., "Nonlinear Estimation Applied to the Nonlinear Inverse Heat Conduction Problem," International Journal of Heat and Mass Transfer, Vol. 13, 1970, pp. 703-716.

8. Beck, J. V., "Criteria for Comparison of Methods of Solution of the Inverse Heat Conduction Problem," Nuclear Engineering and Design, Vol. 53, No. 1, June 1979, pp. 11-22.

9. Muzzy, R. J., J. H. Avila, and D. E. Root, "Topical Report: Determination of Transient Heat Transfer Coefficients and the Resultant Surface Heat Flux from Internal Temperature Measurements," GEAP-20731, General Electric Co., San Jose, California, January 1975.

10. Bass, B. R., "Application of the Finite Element Method to the Nonlinear Inverse Heat Conduction Problem Using Beck's Second Method," ASME Paper No. 78-WA/TM-1, 1978 (to be published in Transactions of ASME, Journal of Engineering for Industry).

11. Imber, M., "Temperature Extrapolation Mechanism for Two-Dimensional Heat Flow," AIAA Journal, Vol. 12, No. 8, August 1974, pp. 1089-1093.

12. Imber, M., "Two-Dimensional Inverse Conduction Problem — Further Observations," AIAA Journal, Vol. 13, No. 1, January 1975, pp. 114-115.

13. Mitchell, A. R. and R. Wait, The Finite Element Method in Partial Differential Equations, John Wiley and Sons, London, 1977.

14. Zienkiewicz, O. C., The Finite Element Method, McGraw-Hill, London, 1977.

15. Bathe, K. J. and E. L. Wilson, Numerical Methods in Finite Element Analysis, Prentice-Hall, Englewood Cliffs, 1976.

16. Ott, L. J. and R. A. Hedrick, "ORTCAL — A Code for THTF Heater Rod Thermocouple Calibration," NUREG/CR-0342, ORNL/NUREG-51, February 1979.

APPENDICES

APPENDIX A

ORMDIN USERS MANUAL

INTRODUCTION

Program ORMDIN is designed primarily to perform a transient two-dimensional nonlinear inverse heat conduction analysis of the THTF bundle 3 heater rod depicted in Figure 7. However, the program can be applied to other cylindrical geometries for which the thermophysical properties are prescribed functions of temperature. The program assumes that discretized temperature histories are provided at three thermocouple locations in the interior of the cylinder, corresponding to the case L = 3 in Section IV.[7] Concurrent with the two-dimensional analysis, ORMDIN also generates one-dimensional solutions for each of the three thermocouple radial planes using a computational model described in Appendix B.

Program ORMDIN uses an in-core solution technique and allocates storage in unlabeled common dynamically during the different phases of the solution. The dimension of unlabeled common is adjusted in program MAIN to provide sufficient storage for the problem under consideration. Storage allocation is checked in each phase of the solution to ensure that the maximum is not exceeded. If sufficient storage is not available, an error message is printed that specifies the required dimension of unlabeled common for that phase of the solution and execution is terminated.

In the user instructions that follow, each card or group of cards is identified by the format used on the card(s), the names of the variables, the meaning of the variables and notes.

---

[7] A second version of ORMDIN has been developed to treat both the cases L = 3 and L = 6.

I. HEADING CARD (10A8)

Notes	Columns	Variable	Entry
	1 - 80	HED(10)	Enter the master heading information for use in labeling the output

II. MASTER CONTROL CARDS

Card 1 (4I5, 2F10.3, 5I5)

Notes	Columns	Variable	Entry
1/	1 - 5	NUMNP1	Total number of nodal points for one-dimensional finite element model
1/	6 - 10	NUMFDN	Total number of nodal points for one-dimensional finite difference model
2/	11 - 15	NUMNP2	Total number of nodal points for two-dimensional finite element model
3/	16 - 20	NSTE	Number of solution time steps
3/	21 - 30	DT	Time step increment
4/	31 - 40	TSTART	Time at solution start
	41 - 45	IPRT	Print control for computed temperatures at nodal points for two-dimensional model EQ.0: Print temperatures only at nodal points in thermocouple radial planes EQ.1: Print temperatures at all nodal points
	46 - 50	IPRD	Print control for input thermocouple temperature data EQ.0: Do not print thermocouple data EQ.1: Print thermocouple data
5/	51 - 55	IPLT	Option to save variables for plotting EQ.0: No EQ.1: Yes
6/	56 - 60	IRINT	Interval for saving restart information EQ.0: Default set to 9999
6/	60 - 65	MODEX	Solution mode EQ.0: Execution EQ.1: Restart

II. MASTER CONTROL CARDS (Contd.)

Card 1 (Contd.)

NOTES/

1/ See Appendix B for a description of the one-dimensional model. NUMNP1 controls the number of Card 6-type cards to be read. NUMFDN controls the number of cell radii read from Card 7.

2/ NUMNP2 controls the number of Card 8-type cards to be read.

3/ The solution domain is determined by [TSTART, TSTART + NSTE*DT].

4/ TSTART is the solution time corresponding to the initial condition. If MODEX.EQ.1, set for a restart, TSTART.EQ.0 can be used and the correct value of TSTART will be read from the restart file.

5/ When IPLT.EQ.1, the solution variables listed below are saved on Units 3 and 4 for each time step. Each record is written using an unformatted WRITE statement.

Unit	Variable	Definition
3	TIME	Time t
	(TCQ(I),I=1,5)	Measured data
	(TEMP(NTCN(J),1),J=1,3)	Computed thermocouple temperatures
	TCTR	Computed center rod temperature
	(TEMP(NN(J),1),J=1,3)	Surface temperature at TC radial planes
	TSA SFA	Average surface temperature and surface flux at TC radial planes
	(SFX(I),I=1,3)	Computed surface flux at TC radial planes
4	TIME	Time t
	(TEMP(LWT(I),1),FLUX(I), I=1,NBP1)	Temperature and heat flux at surface nodes
	(TEMP(ID(I),1),I=1,NP)	Nodal temperatures

II. MASTER CONTROL CARDS (Contd.)

Card 1 (Contd.)

6/ When restart information is being saved every IRINT time steps, the restart information from the last save is overwritten. Unit 2 serves as the output file for saving information. To execute the program in restart mode, set MODEX.EQ.1 and change the JCL so that the Unit 2 output from the previously saved solution can be read by the program from Unit 1.

Card 2 (3I5, F10.4)

Notes	Columns	Variable	Entry
	1 - 5	ISREFK	Number of time steps between reformation of conductivity matrix. Every ISREFK steps, a new [S] matrix is formed (see equation (16)) EQ.0: Default, set to "1"
	6 - 10	IEQUIT	Number of time steps between equilibrium iterations (see equations (14) - (17)) EQ.0: Default, set to "1"
	11 - 15	ITEMAX	Maximum number of equilibrium iterations permitted (see equations (15), (16), (18)) EQ.0: Default, set to "15"
	16 - 25	TOL1	Relative tolerance used to measure equilibrium convergence (see equation (19)) EQ.0: Default, set to "1.E-3"

Card 3 (3I5) Nodal Temperature Printout Card

Notes	Columns	Variable	Entry
1/	1 - 5	NPB(1)	Number of nodes in radial plane 1 for condensed printout
	6 - 10	NPB(2)	Number of nodes in radial plane 2 for condensed printout
	11 - 15	NPB(3)	Number of nodes in radial plane 3 for condensed printout

II. MASTER CONTROL CARDS (Contd.)

Card 3 (Contd.)

NOTES/

1/ These nodes of the 2-D model are selected near a thermocouple radial plane to give a condensed printout of the radial plane temperature profile for easy comparison with the 1-D model profile.

Card 4 (3I5, 3F10.0) Inverse Control Card

Notes	Columns	Variable	Entry
1/	1 - 5	KTER	Maximum number of iterations permitted on surface heat flux q (see equation (32))
	6 - 10	NLAG	Number of time steps used in analysis interval (parameter "J" of equation (27)) (NLAG.GE.1)
2/	11 - 15	ISF2	Mode of initializing 2-D surface flux vector q EQ.0: 1-D approximation EQ.1: 2-D extrapolation
3/	16 - 25	BETA	Factor used to increment q in the advanced time intervals, equation (25)
4/	26 - 35	TOL2	Convergence tolerance for heat flux, inequality (35)
5/	36 - 45	EPSH	Perturbation factor for heat flux (parameter λ of equation (30))

NOTES/

1/ KTER is the maximum number of iterations allowed in the minimization procedure for the sum of squares function of equation (27). If the index H of equation (32) exceeds KTER, a message is printed and execution is terminated.

2/ If ISF2.EQ.0, the heat flux vector q computed by the 1-D model is used as the first approximation in the subsequent 2-D calculation. If ISF2.EQ.1, and this is the recommended option, the vector q is approximated by a linear extrapolation of the 2-D solutions in the previous time steps according to equations (24) - (26).

II. MASTER CONTROL CARDS (Contd.)

Card 4 (Contd.)

3/ For the model of Figure 8, BETA.EQ.0.5 is recommended.

4/ For the model of Figure 8, TOL2.EQ.0.05 is recommended.

5/ For the model of Figure 8, EPSH.EQ.1.E-3 is recommended.

III. NODAL POINT DATA

Card 5 (6I5)

Notes	Columns	Variable	Entry
	1 - 5	NTCN(1)	2-D global node number of thermocouple in radial plane 1
	6 - 10	NISE(1)	2-D global node number of surface heat flux node in radial plane 1
	11 - 15	NTCN(2)	Plane 2, etc.
	16 - 20	NISE(2)	
	21 - 25	NTCN(3)	Plane 3, etc.
	26 - 30	NISE(3)	

Card 6 (A1, I4, A1, I4, 2F10.0, I5) 1-D Nodal Point Data for Finite Element Discretization

Notes	Columns	Variable	Entry
1/	1	IT	Symbol describing the coordinate system for node N EQ. : Cartesian (X, Y, Z) EQ.X: X-cylindrical
	2 - 5	N	Node number; GE.1 and LE.NUMNP1 (see Card 1)
	6	JPR	Print suppression flag (ignored unless N.EQ.1) EQ. : No suppression EQ.A: Suppress ordered list of node coordinates EQ.B: Suppress list of equation numbers EQ.C: Both A and B above

III. NODAL POINT DATA (Contd.)

Card 6 (Contd.)

Notes	Columns	Variable	Entry
2/	7 - 10	ID(N)	Leave blank
	11 - 20	Y(N)	Radial coordinate of 1-D finite element node (inches)
	21 - 30	Z(N)	Leave blank
3/	31 - 35	KN	Node number increment for nodal data generation EQ.0: No generation

NOTES/

1/ The X-cylindrical coordinate system has coordinate pairs (r,θ), see Figure 4.

2/ The correct values for ID are computed internally in the program.

3/ If the sequence of node numbers N being input by cards has missing numbers and KN is specified as positive, then the program will generate nodes by linear interpolation between the nodes bracketing the missing sequence. Node numbers will be assigned to these nodes by incrementing from the first node number in the sequence in steps of KN. Fewer input cards are thus required.

Card 7 (8F10.5)

Notes	Columns	Variable	Entry
1/	1 - 10	RC(2)	Radius of finite difference cell 2 (inches)
	11 - 20	RC(3)	Radius of finite difference cell 3
		etc.	
		RC(N)	Radius of finite difference cell N.EQ. NUMFDN + 2

NOTES/

1/ See Appendix B for a description of the one-dimensional finite difference model.

III. NODAL POINT DATA (Contd.)

Card 8 (A1, I4, A1, I4, 2F10.0, I5) 2-D Nodal Point Data

Notes	Columns	Variable	Entry
1/	1	IT	Symbol describing the coordinate system for this node EQ. : Cartesian (X, Y, Z) EQ.X: X-cylindrical
1/	2 - 5	N	Node number G E.1 and LE NUMNP2
1/	6	JPR	Print suppression flag (ignored unless N.EQ.1) EQ. : No suppression EQ.A: Suppress ordered list of node coordinates EQ.B: Suppress list of equation numbers EQ.C: Both A and B above
1/	7 - 10	ID(N)	Leave blank
1/	11 - 20	Y(N)	X (or r) coordinate (inches)
	21 - 30	Z(N)	Y (or θ) coordinate
1/	31 - 35	KN	Node number increment for node data generation EQ.0: No generation

NOTES/

1/ See notes for Card 6.

Card 9 (16I5) Thermocouple Radial Plane Nodes Card

Notes	Columns	Variable	Entry
1/	1 - 5	IAZ(1,1)	Global node number of the first node on radial plane 1
	6 - 10	IAZ(2,1)	Global node number of the second node on radial plane 1
		etc.	Continuing on next card if necessary
1/	1 - 5	IAZ(1,2)	Global node number of the first node on radial plane 2
		etc.	as above

III. NODAL POINT DATA (Contd.)

Card 9 (Contd.)

Notes	Columns	Variable	Entry
1/	1 - 5	IAZ(1,3)	Global node number of the first node on radial plane 3
		etc.	as above

NOTES/

1/ The program expects to read NPB(I) nodal points for radial plane I, I = 1, 3, as described in the notes for Card 3.

IV. ELEMENT DATA

Card 10 (I5) One-Dimensional Elements Card

Notes	Columns	Variable	Entry
1/	1 - 5	NUME1	Number of elements in 1-D model

NOTES/

1/ NUME1 is the number of elements in the 1-D finite element model described in Appendix B.

Card 11 (6I5) Individual 1-D Element Card

Notes	Columns	Variable	Entry
1/	1 - 5	M	1-D conduction element number
1/	6 - 10	II	Left node number
1/	11 - 15	JJ	Right node number
2/	16 - 20	MTYP	Material type
3/	21 - 25	KG	Node generation increment for missing element
	26 - 30	KQ	Internal heat generation flag EQ.0: No internal heat generation EQ.1: Yes

IV. ELEMENT DATA (Contd.)

Card 11 (Contd.)

NOTES/

1/ The one-dimensional finite element conduction model is described in Appendix B.

2/ The variable MTYP describes the material from the material model library listed below that is used to determine thermophysical properties for the element M.

Material Model Library:

MTYP	Material
1	Annular boron nitride
2	Core boron nitride
3	Chromel-alumel
4	Inconel 600
5	Magnesium oxide (80% theoretical density)
6	316 stainless steel
7	TC composite I (junction)
8	TC composite II (nonjunction)
9	TC composite III (center grouping)
10	User defined material

Optimum polynomial functions of temperature for the heat capacity and thermal conductivity of material models 1 through 9 have been incorporated into ORMDIN. For material models 1 and 2 (annular and core boron nitride), the effective thermal conductivity must be determined *in situ* as part of a rod calibration procedure described in Reference [16]. The coefficients obtained from this calibration procedure are input on Cards 20 and 21. Material model 10 is included to permit the user to input temperature function data for heat capacity and thermal conductivity on Cards 22 - 25.

3/ Elements must be input in increasing element number order. If cards for elements (M + 1, M + 2, ..., M + J) are omitted, these "J" missing elements are generated using MTYP of element "M" and by incrementing the node numbers of successive elements with the value "KG"; KG is taken from the first card of the element generation sequence (i.e., from the "Mth" element card).

IV. ELEMENT DATA (Contd.)

Card 12 (16I5) (Skip if NUMFDN.EQ.0 on Card 1)

Notes	Columns	Variable	Entry
1/	1 - 5	MATFD(3)	Material model for cell 3 of the finite difference model
	6 - 10	MATFD(4)	Material for cell 4
		etc.	
		MATFD(NUMFDN + 2)	Material model for the outermost cell

NOTES/

1/ See Note 2 of Card 11 for a description of different material types and see Appendix B for a description of the finite difference model.

Card 13 (8I5) Two-Dimensional Elements Card

Notes	Columns	Variable	Entry
1/	1 - 5	NUME2	Number of 2-D conduction elements
2/	6 - 10	ITYP2D	Type of element EQ.0: Axisymmetric EQ.1: Plane
3/	11 - 15	MXNODS	Maximum number of nodes per element, 2-D model
4/	16 - 20	NINT	Numerical integration order NINT.GE.1 and LE.3
	21 - 25	NBYE	Total number of elements with surface boundary
5/	26 - 30	NBND	Total number of nodes on the surface boundary with prescribed heat flux
6/	31 - 35	NSST	Number of constrained nodes
7/	36 - 40	INTR	Boundary interpolation option EQ.0: Linear EQ.1: Nonlinear

IV. ELEMENT DATA (Contd.)

Card 13 (Contd.)

NOTES/

1/ Two-dimensional conduction element numbers begin with "1" and end with the total number NUME2 of conduction elements.

2/ Use ITYP2D.EQ.1.

3/ MXNODS limits the number of nodes that can be used to describe any of the elements in this group. A minimum of 4 and a maximum of 8 nodes can be used with the 2-D elements.

4/ For rectangular elements, an integration order of 2 is suggested. If the elements are distorted, an integration order of 3 should be used.

5/ NBND is set equal to the total number of nodes of the finite element model that are positioned on the surface of the rod.

6/ To generate the initial steady-state solution, the temperature must be constrained at one or more nodes. In the 2-D model, NSST nodes near the center of the rod are constrained to be equal to the initial center thermocouple temperature. The constrained node numbers are entered on Card 16.

7/ Surface flux boundary conditions are computed by interpolating the values of the surface flux q_ℓ, ℓ = 1, 2, 3, at radial plane surface nodes. If INTR.EQ.0, the flux values q_ℓ are interpolated linearly. If INTR.EQ.1, the interpolation described by equation (37) is used.

Card 14 (5I5) Individual 2-D Element Card

Notes	Columns	Variable	Entry
1/	1 - 5	M	2-D conduction element number
2/	6 - 10	IEL	Number of nodes used to describe this element
3/	11 - 15	MTYP	Material type (add 100 if surface element)
1/	16 - 20	KG	Node generation increment for missing elements

IV. ELEMENT DATA (Contd.)

Card 14 (Contd.)

Notes	Columns	Variable	Entry
	21 - 25	KQ	Internal heat generation flag EQ.0: No internal heat generation EQ.1: Yes

NOTES/

1/ Elements must be input in ascending element number order. If data cards for elements (M + 1, M + 2, ..., M + J) are omitted, these "J" missing elements are generated using IEL and MTYP given on the card for element "M" and by incrementing node numbers of successive elements with the value "KG". The value of KG used for incrementation is taken from the Mth element card, and only the nonzero nodes appearing on the Mth element card are incremented when generating element data. The last element in the group cannot be generated and must be input.

2/ The number of nodes of element "M" is defined by "IEL". However, all 8 entries from NOD(I) on Card 15 are read; if IEL.LT.8, the particular node locations not used in this element, need to be input as "0" in NOD(I). Figure 18 defines the input sequence that must be observed for element node input.

3/ See Note 2 of Card 11 for the available material types. If this element has an external boundary, add 100 to the value of MTYP.

Card 15 (8I5) Element Connectivity Card

Notes	Columns	Variable	Entry
1/	1 - 5	NOD(1)	Global node number for element node 1 of element M from Card 14
	6 - 10	NOD(2)	Global node number for element node 2
		etc.	
	36 - 40	NOD(8)	Global node number for element node 8

NOTES/

1/ See Figure 18 and Notes 1 and 2 of Card 14.
IMPORTANT: Nodes 1, 2 (and 5, if included) must represent the surface nodes for those elements having an external boundary.

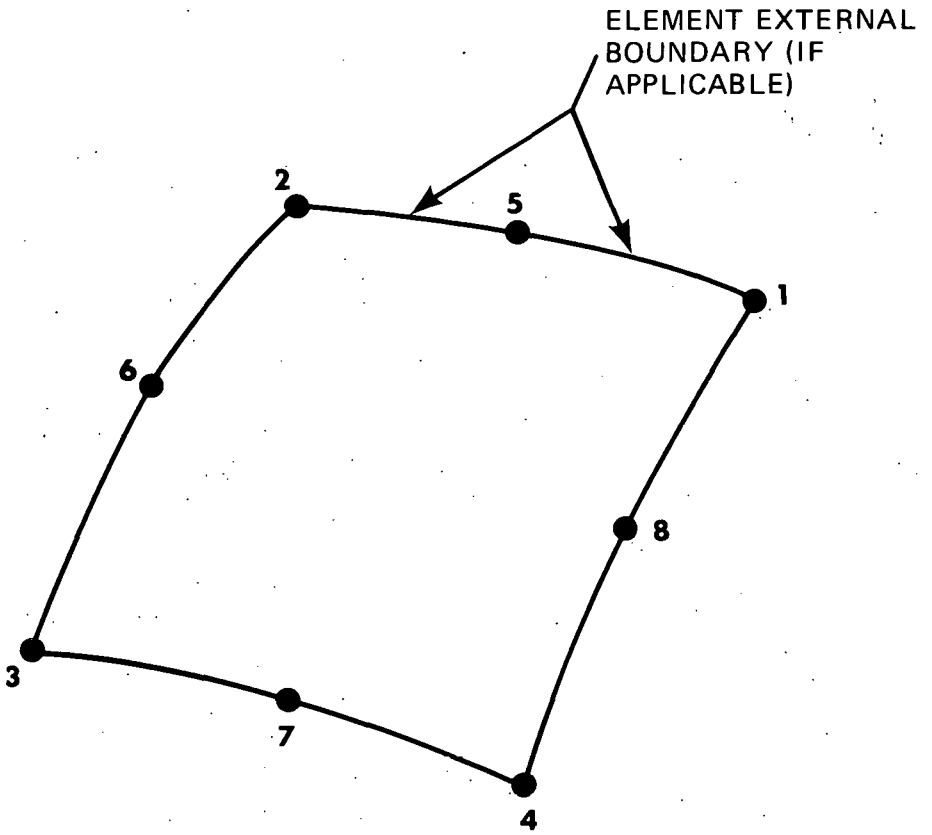

Figure 18. Element node number input sequence for 2-D conduction elements

IV. ELEMENT DATA (Contd.)

Card 16 (16I5) Constrained Nodes Card

Notes	Columns	Variable	Entry
1/	1 - 5	LNST(1)	Temperature constrained node
	6 - 10	LNST(2)	Temperature constrained node
		etc.	
		LNST(NSST)	Temperature constrained node

NOTES/

1/ See Note 6 on Card 13.

V. TIME FUNCTION DATA

Card 17 (2I5)

Notes	Columns	Variable	Entry
1/	1 - 5	NPTM	Total number of points used to input the thermocouple data and internal heat generation data
1/	6 - 10	NUNIT	I/O unit for input of time function curves

NOTES/

1/ NPTM describes the total number of points (i.e., $[t_i$, $T_\ell^P(t_i)$, $Q(t_i)]$ triplets) which define the time-thermocouple temperature functions $T_\ell^P(t)$ of the inverse analysis and the time-internal heat generation function Q(t). NUNIT is the I/O unit number for the input of these data. NUNIT.EQ.5 is used for card input.

Card 18 (2F10.0)

Notes	Columns	Variable	Entry
1/	1 - 10	RI	Inner radius of heater annulus (inches)
	11 - 20	RO	Outer radius of heater annulus (inches)

V. TIME FUNCTION DATA (Contd.)

Card 18 (Contd.)

NOTES/

1/ These radii are used to compute a density term for calculation of heat generation from the Q values input on Card 19. See Note 1 of Card 17 for related information.

Card 19 (6F10.0 if NUNIT = 5; otherwise, unformatted)
Time Function Data Card

Include one card for each point I = 1, 2, ..., NPTM

Notes	Columns	Variable	Entry
1/	1 - 10	TIMV(I)	Time of measurement I (seconds)
	11 - 20	RV(1,I)	Data for thermocouple 1 (deg F)
	21 - 30	RV(2,I)	Data for thermocouple 2
	31 - 40	RV(3,I)	Data for thermocouple 3
	41 - 50	RV(4,I)	Data for center thermocouple
	51 - 60	RV(5,I)	Heat generation rate (Btu/hr-ft)

NOTES/

1/ The following units are assumed for each input variable:

Time - second
Temperature - degree F
Heat generation rate - BTU/hour/linear foot of heater rod

See Note 1 of Card 17 for related information.

VI. MATERIAL MODEL DATA

Card 20 (3F15.5) Material Model 1: Thermal conductivity coefficients for annular boron nitride
(Leave this card blank if material model 1 is not used)

Notes	Columns	Variable	Entry
1/	1 - 15	CBNANN(1)	Coefficients of temperature-thermal conductivity function for annular boron nitride
	16 - 30	CBNANN(2)	
	31 - 45	CBNANN(3)	

VI. MATERIAL MODEL DATA (Contd.)

Card 20 (Contd.)

NOTES/

1/ The coefficients of the thermal conductivity function for annular boron nitride are determined *in situ* as part of the heater rod calibration procedure described in Reference [16].

Card 21 (3F15.5) Thermal conductivity coefficients for core boron nitride
(Leave this card blank if material model 2 is not used)

Notes	Columns	Variable	Entry
1/	1 - 15	CBNCOR(1)	Coefficients of temperature-thermal conductivity function for core boron nitride
	16 - 30	CBNCOR(2)	
	31 - 45	CBNCOR(3)	

NOTES/

1/ The comments of Note 1, Card 20, also apply to the core boron nitride material model 2.

Card 22 (2I5) Control card for material model 10 (user-supplied model)
(Leave card blank if material model 10 is not used)

Notes	Columns	Variable	Entry
1/	1 - 5	NCRHO	Total number of points (i.e., $[T_i,c_i]$ pairs) used to input the temperature-specific heat function c(t) (NCRHO.LE.25)
1/	6 - 10	NAK	Total number of points (i.e., $[T_i,k_i]$ pairs) used to input the temperature-thermal conductivity function k(T) (NAK.LE.25)

NOTES/

1/ The specific heat and thermal conductivity are temperature dependent and are described by the discrete points entered on Cards 23 and 24.

VI. MATERIAL MODEL DATA (Contd.)

Card 23 (2F10.3) Temperature function data for specific heat of material model 10
(Skip this card if NCRHO.EQ.0)

Notes	Columns	Variable	Entry
1/	1 - 10	TCRHO(I)	Temperature at point, I, T_I
1/	11 - 20	CRHO(I)	Function value of specific heat at point I, $c(T_I)$

NOTES/

1/ Linear interpolation is used to compute the specific heat between the points input on this card. A total of NCRHO cards must be input, with temperature values TCRHO(I) in ascending order. The temperature interval (TCRHO(1), TCRHO(NCRHO)) must contain all computed temperatures of the solution.

Card 24 (2F10.3) Temperature function data for thermal conductivity of material model 10
(Skip this card if NAK.EQ.0)

Notes	Columns	Variable	Entry
1/	1 - 10	TAKINP(I)	Temperature at point I, T_I
1/	11 - 20	AKINP(I)	Function value of thermal conductivity at point I, $k(T_I)$

NOTES/

1/ The general restrictions of Card 23 also apply to Card 24.

Card 25 (F10.3) Density of material model 10
(Skip this card if NCRHO.EQ.0)

Notes	Columns	Variable	Entry
	1 - 10	DIN	Density ρ of material model 10

This concludes the card input to the program.

APPENDIX B

ONE-DIMENSIONAL COMPUTATIONAL MODEL OF THE ELECTRIC HEATER ROD

The one-dimensional computational model of the electric heater rod utilizes a combined finite element and finite difference discretization. In Figure 19, the region $r \leq r^P$ of the rod is partitioned by a set of one-dimensional linear isoparametric elements (the finite element model is described in [3]). The input thermocouple data $T^P(t)$ is used as a conventional boundary condition in this finite element formulation to determine the temperature solution $T(r,t)$ for $r \leq r^P$. To compute the solution in the region $r^P < r \leq a$, the finite difference discretization described in [2] is "grafted" onto the finite element model (FEM) at the outermost nodes NUMNP1-1, NUMNP1 (NUMNP1 is entered on Card 1). The finite difference model (FDM) consists of NTC = NUMFDN + 2 cells (NUMFDN is entered on Card 1), with the nodes for cells 1,2 of the FDM coinciding with nodes NUMNP1-1, NUMNP1 of the FEM. The cell radii $r_2, r_3, \ldots, r_{NTC}$ and cell material models are specified by the user on Card 7 and Card 12, respectively; each cell consists of only one material model. From Chapter II of [2], the cell radius r_1 is computed by the program from

$$r_1^2 = 2\bar{r}_2^2 - r_2^2 \quad , \tag{B1}$$

and the remaining nodal radii $r_3, r_4, \ldots, r_{NTC}$ from

$$\bar{r}_{I+2}^2 = \frac{1}{2}(r_{I+2}^2 + r_{I+1}^2) \quad , \tag{B2}$$

I = 1, NUMFDN.

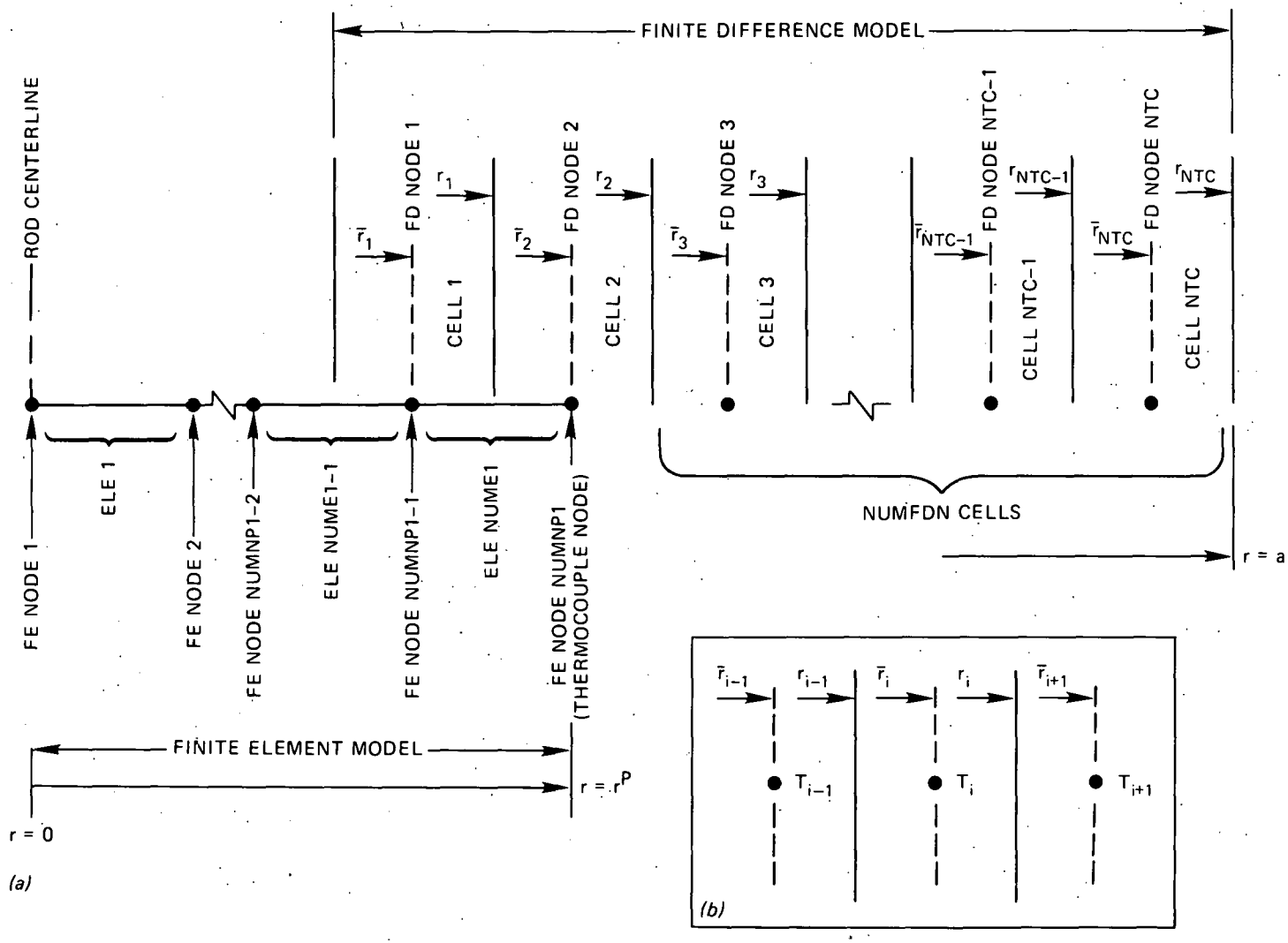

Figure 19. One-dimensional discretization of heater rod
(a) 1-D model
(b) typical cell

For a given time $(i)\Delta t$, it is assumed that the temperatures at all nodes of the one-dimensional model are known. To determine the values at time $(i+1)\Delta t$, the FEM is first solved using the boundary condition $T_{(i+1)\Delta t}$ at $r = r^{P}$. With the temperatures at the FDM nodes 1,2 thus determined, the (P)th iterative estimate of the remaining nodal values is computed from the equation (see Figure 19-b)

$$b_{I+1}^{(P-1)}\, T_{I+1;(i+1)\Delta t}^{(P)} = -\, d_I^{(P)}\, T_{I;(i)\Delta t} - b_{I-1}^{(P)}\, T_{I-1;(i+1)\Delta t}^{(P)} + \left(b_I^{(P)} + d_I^{(P)} + b_{I+1}^{(P-1)}\right) T_{I;(i+1)\Delta t}^{(P)} \,,$$

$$I = 2,\ NTC-1 \qquad \text{(B3)}$$

which is derived from equations B.9 of [2]. The temperature-dependent coefficients in (B3) are given by

$$b_{I+1} = \frac{2}{\dfrac{\ell n(\bar{r}_{I+1}/r_I)}{k_{I+1}} + \dfrac{\ell n(r_I/\bar{r}_I)}{k_I}} \qquad \text{(B4)}$$

$$b_{I-1} = \frac{2}{\dfrac{\ell n(\bar{r}_I/r_{I-1})}{k_I} + \dfrac{\ell n(r_{I-1}/\bar{r}_{I-1})}{k_{I-1}}} \qquad \text{(B5)}$$

$$d_I = \frac{\rho c_I (r_I^2 - r_{I-1}^2)}{\Delta t} \qquad \text{(B6)}$$

The estimate for the FDM nodal temperatures $T_3, \ldots, T_{NTC}$ is corrected iteratively using (B3) until the incremental change in temperatures satisfies a convergence criterion analogous to that of equation (19).

Finally, the surface heat flux is approximated from the relation

$$2aq_{(i+1)\Delta t} = b_{NTC-1}(T_{NTC;(i+1)\Delta t} - T_{NTC-1;(i+1)\Delta t}) - d_{NTC}(T_{NTC;(i+1)\Delta t} - T_{NTC;(i)\Delta t}) \quad , \tag{B7}$$

which is derived from equation B.69 of [2]. The surface temperature is calculated from equation B.72 of [2], which is given by

$$T_{SURF;(i+1)\Delta t} = T_{NTC;(i+1)\Delta t} - \frac{2aq_{(i+1)\Delta t}}{\frac{2k_{NTC}}{\ell n(r_{NTC}/\bar{r}_{NTC})}} \tag{B8}$$

When ISF2 = 0 is entered on Card 4, the surface flux values computed from equation (B7) at the three thermocouple radial planes are used as initial estimates in the two-dimensional discretization given by equation (23).

NUREG/CR-1709
ORNL/NUREG/CSD/TM-17
Dist. Category R2

INTERNAL DISTRIBUTION

1. T. M. Anklam
2-4. B. R. Bass
5. M. Bender
6. H. P. Carter/A. A. Brooks/ CSD Library
7. K. W. Childs
8-9. W. G. Craddick
10. R. D. Dabbs
11-13. J. B. Drake
14. G. J. Farris
15. R. M. Flanders
16. M. H. Fontana
17. U. Gat
18. R. C. Hagar
19. C. R. Hyman
20. S. K. Iskander
21. D. G. Morris
22. C. B. Mullins
23. F. R. Mynatt
24. D. S. Napolitan
25-29. L. J. Ott
30. R. E. Textor
31. W. D. Turner
32. J. D. White
33. M. D. White
34. G. L. Yoder
35. Patent Office
36. Central Research Library
37. Document Reference Section - Y-12
38. Engineering Physics Information Center
39-41. Laboratory Records Department
42. Laboratory Records (RC)
43. ORGDP CSD Library
44. ORGDP Library
45. ORGDP Plant Records

EXTERNAL DISTRIBUTION

46-47. Director, Division of Reactor Safety Research, Nuclear Regulatory Commission, Washington, DC 20555
48. Office of Assistant Manager for Energy Research and Development, Department of Energy, Oak Ridge Operations, Oak Ridge, TN 37830
49. A. W. Serkiz, Separate-Effects Research Branch, Mail Stop 1130SS, U. S. Nuclear Regulatory Commission, Washington, DC 20555
50-51. Technical Information Center, DOE
52-436. Given distribution as shown under category R2 (10 copies — NTIS)

☆ U.S. GOVERNMENT PRINTING OFFICE: 1980-740-062/370